Modeling Differential Charging of Composite Spacecraft Bodies Using the Coliseum Framework

Alexander Barrie

Thesis submitted to the faculty of the
Virginia Polytechnic Institute and State University
in partial fulfillment of the requirements for the degree of

Master of Science
in
Aerospace Engineering

Joseph Wang, Committee Chair
Wayne Scales, Committee Member
Rakesh Kapania, Committee Member

August 14, 2006
Blacksburg, Virginia

Keywords: spacecraft charging, particle in cell, electric propulsion plume

Modeling Differential Charging of Composite Spacecraft Bodies Using the Coliseum Framework

Alexander Barrie

Abstract

The COLISEUM framework is a tool designed for electric propulsion plume interactions. Virginia Tech has been developing a module for COLISEUM called DRACO, a particle-in-cell based code capable of plume modeling for geometrically complex spacecraft. This work integrates a charging module into DRACO. Charge is collected via particle impingement on the spacecraft surface and converted to potential. Charge can be stored in the surface, or added to a local ground potential. Current can flow through the surface and is governed by the internal electric field in the spacecraft.

Several test cases were run to demonstrate the code's capabilities. The first was a plume impingement of a composite spherical probe by a xenon thruster. It was shown that the majority of current conducted will reach the interior of the spacecraft, not other surface elements. A conductive interior will therefore result in a uniform surface potential, even for low surface conductivities. A second test case showed a composite spacecraft exposed to a solar wind. This test showed that when a potential gradient is applied to a conductive body, the ground potential of the spacecraft will lower significantly to compensate and maintain a zero net current. The case that used the semiconductive material showed that the effect of the potential gradient can be lowered in cases such as this, where some charge will always be stuck in the surface. If a dielectric material is used, the gradient will disappear altogether. The final test case showed the effect of charge exchange ion backflow on the potential of a spacecraft similar to the DAWN spacecraft. This case showed that CEX ion distribution is not even along the spacecraft and will result in a transverse potential gradient along the panel.

Contents

List of Tables

List of Figures

Acknowledgments

Many people helped me with this project and are worthy of recognition. Following, are a few of these individuals, but by no means all of them.

First, I would like to thank Dr. Joseph Wang, my faculty advisor. He helped me get accepted to graduate school and guided me through the research process. He was responsible for keeping me on the right track with his knowledge of spacecraft and plasmas, and helped me prepare my research in a professional and correct way.

Dr. Wayne Scales, was also instrumental in my research. His expertise in electromagnetism proved invaluable when deriving the governing equations of spacecraft surface charging. I would also like to thank Dr. Rakesh Kapania for his willingness to serve on my committee and for his questions and critiques of this work.

Lubos Brieda, one of the earlier designers of the DRACO code, provided invaluable support in getting my simulations to run in DRACO. Few people have as much knowledge into the inner workings of DRACO, with all of its idiosyncrasies and caveats. This work would never have been completed

without many hours on the phone and email with Lubos.

Next, I would like to acknowledge the rest of the CAPLab team at Virginia Tech for bouncing ideas off of, making the lab enjoyable, and griping about work.

I would like to thank the Air Force Research Lab (AFRL) for providing funding for the DRACO project which allowed me to do my work. In a similar note, I would like to thank Dr. Robert Walters and the AOE department at Virginia Tech for funding me to work with the departments SGI system.

Joe Gleason helped through a variety of C++ problems and helped me to develop several JAVA programs to convert data between formats. This saved me a large amount of time when developing my codes.

I would like to pay special attention to Luke Scharf, the AOE department's system administrator. He had about a hundred vastly different systems to maintain and did so with skill. He helped me through all kinds of compiler errors, program errors, licensing issues, and assorted other computer problems. He will be sorely missed by me and the entire department as he leaves to work on System X.

Finally, I would like to thank my family and friends for supporting me through this entire process. I could not have gotten through it all without you guys.

Chapter 1

Introduction

Spacecraft charging[5, 6] is an important aspect of spacecraft environment interactions. Spacecraft have no way to electrically ground themselves, therefore the potential of a spacecraft is determined by charge collected from its environment. When materials are conductive, the charge will distribute and elevate the overall ground potential of the spacecraft. Studies into spacecraft charging from the ambient plasma environment began in the 1950s[5] and the physics behind it is now well understood[7]. Studies into spacecraft charging effects from artificial plasma sources have only recently been undertaken, and the underlying physics is still being investigated. The purpose of this work is to develop a charging model for studying the charging effects induced on a spacecraft from plasma induced by an electric propulsion device.

Electrostatic thrusters propel charged particles in order to generate thrust. Most of these particles will stay in a tight beam and will never affect the

spacecraft. Some particles however, will collide with neutral particles and form charge exchange ions. These charge exchange, or CEX ions can backflow towards the spacecraft and impart a current to the surface[8]. The CEX plasma is the dominant current source to spacecraft using electrostatic propulsion, however additional current sources can be created through a variety of surface interactions such as photoelectron emission[9, 10] and secondary emissions[11].

The effects of spacecraft charging are dependent on the surface material properties. When materials are nonconductive, such as glass, current will not flow over the surface and potential gradients, or differential charging, can occur. When a differential charge gradient becomes too high, arcing can occur. Arcing can have substantial effects on the arc points, frying electronics or burning holes in a structural element[12]. Often times, materials can be designed and installed in such a way as to minimize differential charging. There are some cases, such as solar panels, however, where this is not an option. Solar panels must be made of specific materials and are covered with glass to allow light through to the interior cells. Solar panels also have driving potential gradients in order to move the current collected by them. These voltage biases can amplify the problems of differential charging in the dielectric material[13]. Arcing on solar panels can cause cracking of the elements[14], which can cause the spacecraft's power systems to fail. Numerous work has been done both experimentally[15, 16] and through modeling[13, 17, 18] to look at the causes and effects of differential charging on solar panels.

1.1 Spacecraft Charging

Research into spacecraft charging effects began with early rocket tests in the 1950s. Probes to measure charge in the ionosphere were launched on sounding rockets in the early 50s. After the launch of Sputnik, charging probes began to be placed on satellites as well. These measurements were limited in the quality of data gained, and took data primarily in the ionosphere[5].

In the 60s, more accurate charging models were developed. Brundin[19] and Bourdeau [20] published papers on the basic physics behind spacecraft charging, modeling photoelectron emissions and secondary electron emissions. Much of their work was an extension of that of Whipple[6].

The design of the Voyager spacecraft in the 1970s included a thorough investigation into charging effects and how they might be mitigated[21]. The SCATHA mission provided information about LEO and GEO plasma environments, which allowed for increased accuracy in contemporary charging models. These results are brought together in a set of NASA Spacecraft Charging Design Guidelines[22].

Focus then began to shift towards internal charging phenomenon. Several spacecraft failures were suspected to have been caused from deep dielectric charging from high energy electrons. The CRRES spacecraft[23] was subsequently launched to conduct a series of experiments of internal charging phenomenon that led to more accurate models. A review of these events can be found in Garrett and Whipple[5, 24, 6].

In recent years, studies have expanded into more areas. Charging effects of extreme environments such as Jovian moons, high voltage systems, large spacecraft and solar sails, and spacecraft with active plasma emission, such as electric propulsion systems are all of interest. Garret discusses these upcoming challenges in his most recent charging review[25].

1.2 Modeling

Computational modeling of charging effects is an imperative part of the spacecraft design process. This section reviews previous work in developing physics based charging models. Most physics based models use the particle in cell, or PIC, method. The PIC method is a way of representing a plasma, and calculating the associated electric field, using a grid made up of cells. The process by which this conversion happens is duscussed in more detail in Birdsall and Langdon's book[26].

1.2.1 NASCAP

One of the first charging codes was NASCAP, which has been steadily improved over a long period of time. Nascap is a spacecraft charging code being developed over many years by Science Applications International Corporation (SAIC), NASA, and the S-Cubed Division of Maxwell Laboratories. The code was initially developed in 1976 with work continuing until 1984, and was used mainly for GEO environments[27]. Many modifications were made

to the code, including capabilities for LEO environments[28].

The original Nascap code became outdated as computers became faster and computational power increased exponentially during the 1990s. This resulted in the release of Nascap-2k [29, 30]. Naskap-2k has modernized the original Nascap code and has added several new modules with increased functionality.

A boundary element model permits implicit treatment of electric fields, and the DynaPAC[31] code deals with external plasmas and has basic PIC capabilities. Nascap has always been the premier toolkit for charging calculations, however it has never had built in functionality to model the surrounding plasma environment as well as other stand alone PIC programs.

1.2.2 Plume/Interaction Codes

Several codes have been developed at universities and other research institutions to model plume interactions. Plume codes are typically developed using the PIC method. Collisions between particles can typically be handled in two ways: direct simulation Monte Carlo (DSMC), or Monte Carlo Collisions (MCC). DSMC is a more accurate method where collisions are modeled directly. Several plume codes, such as those developed by Boyd[33], Oh[34, 35] and VanGilder[36] use the PIC-DSMC approach to modeling plasma flow. The Aquila module in the COLISEUM framework[37] uses the DSMC collision model as well. MCC is a simpler, approximate method to determine the collision rates. It has been used in codes developed by Koo and Boyd[38] and

is the primary model used in the DRACO module for the coliseum framework that. This work uses the DRACO module, and therefore utilizes the MCC collision model. The physics model and heritage code that DRACO was based on written by Wang et al.[39] is the only in flight data validated model published so far.

EPIC[32] is another module being developed by SAIC. It has capabilities for some 3D interactions, an object toolkit, and a plume tool. The object toolkit allows for an interactive environment in which to create spacecraft models. The plume tool allows for the use of plume's from electric thrusters to be incorporated. The main advantage of EPIC is that it can communicate with Nascap via SOAP (Simple Object Access Protocol), allowing for one large package. The main downside of EPIC is that the plume tool is only 2D. This is fine for axisymetric cases, however there are many cases that cannot be defined in an axisymetric way. As with the other NASCAP modules, additional communication and sharing of information is also required which can slow down simulations.

1.2.3 Recent Comprehensive Models

Many research codes are being developed specific to spacecraft plasma interactions involving electric propulsion. One example of this is SMART-PIC[40, 41], which used data gathered from the SMART-1[42] mission to validate simulation results.

Parallel computing has allowed for large domain and high particle count

simulations such as those performed by Wang[43, 4]. The rapid advance in computer technology has also allowed for advanced multifunction toolkits to be developed such as NASCAP[29, 30], SPIS[44, 45], and COLISEUM[37]. SPIS, or Spacecraft Plasma Interaction Software, has been under development by the ESA. As it is not widely used in the United States, it will not be focused on here. COLISEUM is a framework for solving plasma simulations with complex spacecraft and is discussed in Chapter 2. This work presents a model for differential charging of composite materials which has been integrated into the COLISEUM framework.

1.3 Organization of Thesis

The remainder of this work will be organized as follows:

Chapter 2 describes the COLISEUM framework that this work is a part of. The overall project is described in detail along with a description of the PIC routines used and a description of the particular PIC module used, DRACO. The mesh generation process of DRACO and the new charging module developed by this work are then discussed.

Chapter 3 introduces the algorithms used for charging calculations in this thesis. The first part shows how particles are correlated to the particular element of impact. The second part examines the current collection methods available. Boltzmann and full PIC are reviewed. The next part discusses how current travels through the surface and how it is converted into a potential

difference. The final part discusses how the time scaling works and how it, along with intelligent initial conditions, can speed up simulations.

The modeling results are presented in Chapter 4. Three test cases were investigated. The first test case examines plume impingement on a spherical probe. The second case looks at a composite spacecraft exposed to a solar wind type plasma. The final test case involves a solar array immersed in a thruster plume.

The final Chapter, Chapter 5.1 has some concluding remarks and future work plans that have not yet been implemented. This is followed by the list of references and appendices.

Chapter 2

Coliseum

2.1 Project

The COLISEUM project is headed by the Air Force Research Lab with contributions from Virginia Tech, MIT, and Michigan, with contributions from Advatech Pacific and Cal Polytech. It is a plasma toolkit that has a variety of modules and is easily expandable. It takes user input of almost any type for object and surface models, sputtering/interaction models, and plasma parameters. A variety of solvers can then be implemented and then results can be outputted in several formats and methods (see Figure 2.1. Some of these modules are discussed in the proceeding sections.

As it can be difficult to perform wide scale experiments in a space environment, many experiments and tests are run in vacuum chambers. Since most experimental data is from vacuum chamber sources, COLISEUM must

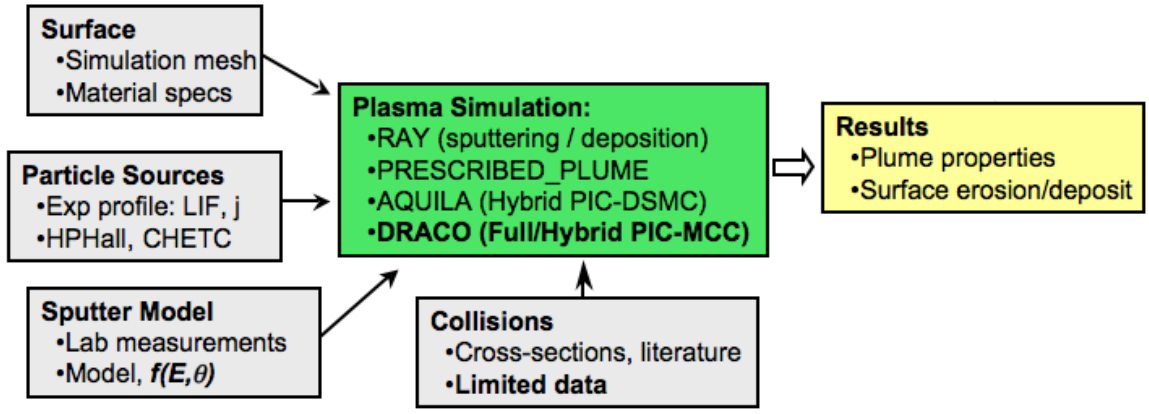

Figure 2.1: Flowchart of the operation of the Coliseum framework

be able to perform vacuum chamber tests as well. COLISEUM therefore supports both open and enclosed domain boundaries, as shown in Figure 2.2.

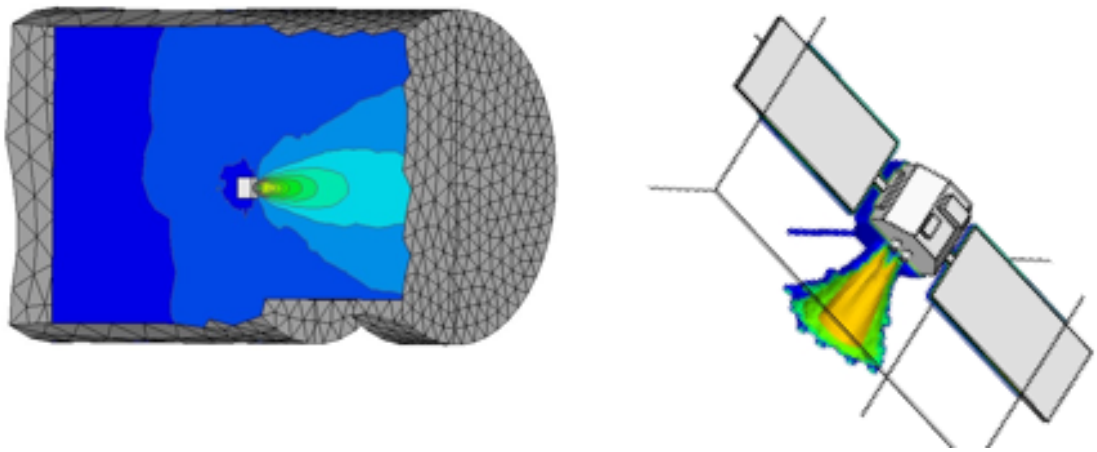

Figure 2.2: Coliseum supports closed as well as open boundaries[1]

The four main plasma modules for COLISEUM are:

- RAY - This is a simple ray tracing algorithm. it is computationally cheap, but not as accurate or powerful as the other options.

- Prescribed-Plume - This code is similar to many other codes and simply has a defined plume. It can be accurate if the plume is well defined, but is still not a very powerful tool.

- AQUILA - This module is being developed by MIT. It utilizes a hybrid PIC-DSMC algorithm with an unstructured mesh. It is largely accurate and can use many types of surfaces.

- DRACO - This module is being developed at Virginia Tech. It can use either a hybrid or full PIC and uses an MCC collision model rather than DSMC. DRACO is further discussed in Section 2.3.

Coliseum uses a set of input files to load in the various parameters for the simulation. They are described below. An example of each is provided in the appendix.

- coliseum.in - Appendix 5.2 - this file provides all the program specifications such as which solvers to use, where to put particle sources, timesteps, which surfaces to load, etc. This is the overall input file with all of the general inputs.

- material.txt - Appendix 5.2 - this file lists all available materials and their associated properties.

- mat_mat.txt - Appendix 5.2 - this file lists available reactions between materials and what should happen when each reaction occurs.
- component.txt - Appendix 5.2 - this file lists all components that make up the simulation and several parameters describing them.
- domain.txt - Appendix 5.2 - this file sets up the simulation domain - cell size, boundary conditions, etc.

2.2 PIC

DRACO utilizes a particle in cell, or PIC, particle movement scheme. PIC is a method of using macroparticles to simulate kinetic processes in plasma. This process involves several steps.

Since computational limitations prevent the modeling of every individual particle, particles can be grouped together into bundles known as macroparticles. Each macroparticle will be the sum of *sw* (specific weight) particles. The PIC simulation will then perform calculations on these macroparticles. From this point, the word particle will refer to a macroparticle.

The first step in the PIC algorithm loop is charge density weighting. The effect of each particle is weighted onto the local grid points on the cartesian mesh. What this means is that a grid point closer to a particle will feel more of that particles influence than one further away. DRACO, for example, uses a linear weighting scheme. Every particle is weighted onto the set of grid points that make up the cell in which the particle resides. This results in a distribution of charge density for each node. Charge density is a measure of how much charge (how many particles) reside at that node. An example of a PIC representation of a plasma is shown in Figure 2.3.

Once the map of charge density is available, Poissons's Equation:

$$-\nabla \cdot \overrightarrow{E} = \nabla^2 \phi = -\frac{\rho}{\epsilon_0} \tag{2.1}$$

can be solved to get an electric field distribution on the grid. There are

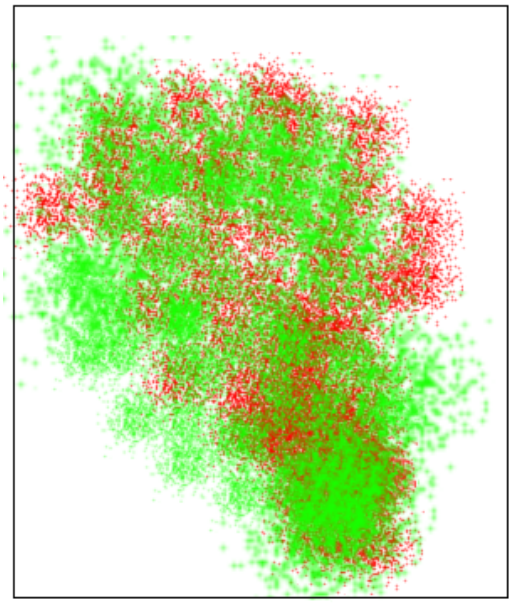

(a) Original plasma

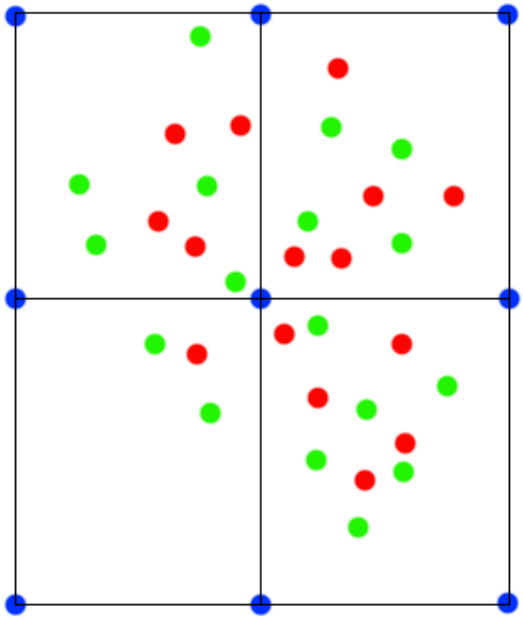

(b) PIC representation

Figure 2.3: A sample two specie plasma as handled in a PIC routine

several solvers available to do this calculation. Each is described in Section 2.3.1. When an electric field is known, the force on each particle can be calculated as the Lorentz Force:

$$\overrightarrow{F} = m\frac{d\overrightarrow{v}}{dt} = q\left(\overrightarrow{E} + \frac{\overrightarrow{v}}{c} \times \overrightarrow{B}\right) \tag{2.2}$$

Once the force on each particle is known, they are moved using the leap frog scheme for the given timestep. The process then repeats and the particles are repositioned. This continues until a steady solution is reached.

2.3 DRACO

DRACO is a 3D, ES-PIC plasma simulation code developed at Virginia Tech. It is based on the plasma simulation code, PLUME[39], developed at NASA for the Deep Space 1 mission by Joseph Wang.

A flowchart of the DRACO module is shown in Figure 2.4. DRACO uses the COLISEUM framework for access to user input and various parameters.

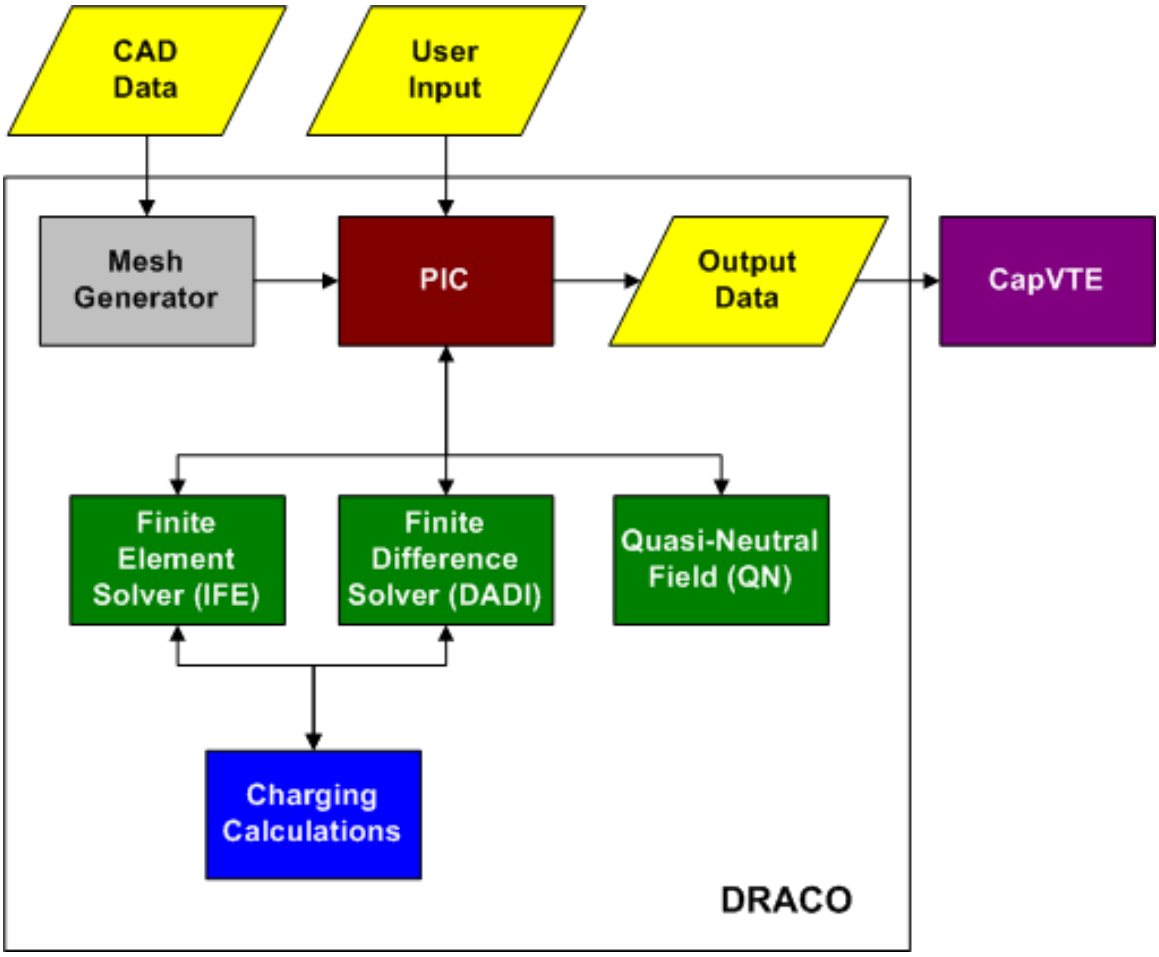

Figure 2.4: Flowchart of the operation of the Draco module

2.3.1 Field Solvers

In an ES-PIC code, the electric field is derived from the Poisson's equation:

$$-\nabla \cdot \overrightarrow{E} = \nabla^2 \phi = -\frac{\rho}{\epsilon_0} \tag{2.3}$$

where $\epsilon_0 = 8.854 \times 10^{-12} F/m$ and is the dielectric permittivity of a free space vacuum.

DRACO has three primary Poisson field solvers available: a quasi-neutral solver, a finite difference solver, and a finite element solver. Each is discussed here.

- Boltzmann - This is the DRACO quasi-neutral solver. This solver assumes that the electrons can be considered a massless fluid. A full fluid model is not implemented, however, It uses a Boltzmann relationship to model the electrons. It uses an inversion of the Boltzmann equation:

$$n_e = n_{e\infty} exp\left(\frac{e\phi}{kT_e}\right) \tag{2.4}$$

  to solve the potential map. This solver is extremely fast, however the Boltzmann solver cannot be used to resolve the sheath and is not valid when positively biased objects exist in the domain. Many of the simulations presented in this work were run with this solver initially in order to resolve the ion positions prior to electrons being introduced.

- DADI - This is a finite difference solver using the Dynamic Alternate-

Direct-Implicit, or DADI, method. It was used in the original PLUME code[39] that DRACO grew out of. It can be run as either a hybrid PIC with particulate ions and fluid electrons, or, as in many cases from this paper, a full PIC which models both electrons and ions as particles. While it is not as computationally fast as the Boltzmann solver, it is more accurate and allows for full PIC simulations. The DADI method is described in detail in Ref. [46].

- Immersed Finite Element - the IFE, or Immersed Finite Element, solver[3] was first written in Fortran by Kafafy et al.[47]. It is the most accurate solver, and is currently the only solver capable of resolving the curvature of surfaces in DRACO.

2.3.2 Mesh

DRACO uses an i, j, k ordered cartesian grid for the storing of plasma parameters. Cells are numbered based on their location. This allows for faster particle movement calculation and access to variables, since there is no calculation involved in transitioning between coordinates and a cell number.

The main disadvantage of using the cartesian mesh is that it can be difficult to translate complex geometries onto a cartesian grid. Points and surfaces will not line up and an algorithm must be put in place to represent a complex, non uniform surface on the cartesian cells. A module called VOLCAR[48] was created to handle this interaction.

Simple shapes can be made to line up exactly with the cartesian mesh, as shown in Figure 2.5. These surfaces are called 'flushed' surfaces, and require no special treatment to align with the cartesian mesh. Often times, the cell size and position are chosen specifically to achieve flushed boundary conditions.

Here, a square is represented on a sample cartesian mesh. The white and tan elements represent exterior elements. They are completely outside the surface and contain only the ambient plasma. The light green elements in the center represent internal elements. These elements are completely inside the surface and contain no particles (particles can occasionally briefly enter internal elements, but are removed at the end of the timestep.) the darker green elements represent boundary elements. These elements are internal to the surface, but they share nodes with exterior elements. These are essentially elements that are on the surface of the object and particles will routinely be passing into these elements as they impact the surface. These impact locations are saved and used for the purposes of surface interaction and charging calculations.

For more complex surfaces to be well defined, the cartesian cells must be broken into smaller segments that can be shaped to match a specified surface. This is done with slices through tetrahedra. Each cell is subdivided into five tetrahedral elements as shown in Figure 2.6. When a surface intersects one of these tetrahedral elements, a slice is made in the element. The overall surface is then defined based on all of these slices through the assorted tetra-

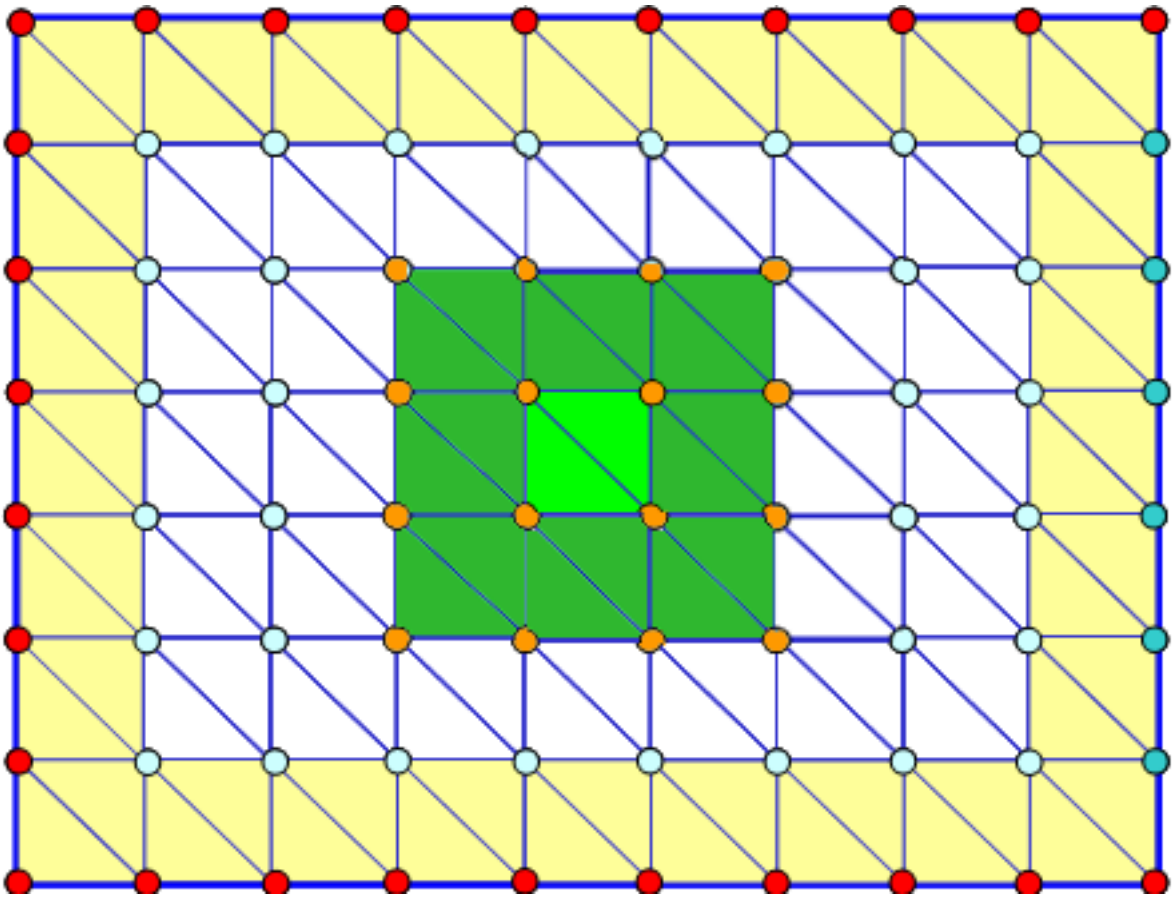

Figure 2.5: Sample grid overlay with flushed boundaries

hedral elements. This allows for reasonable accuracy to be maintained when importing complex shapes into DRACO. For a more detailed description of this process, see Ref. [2].

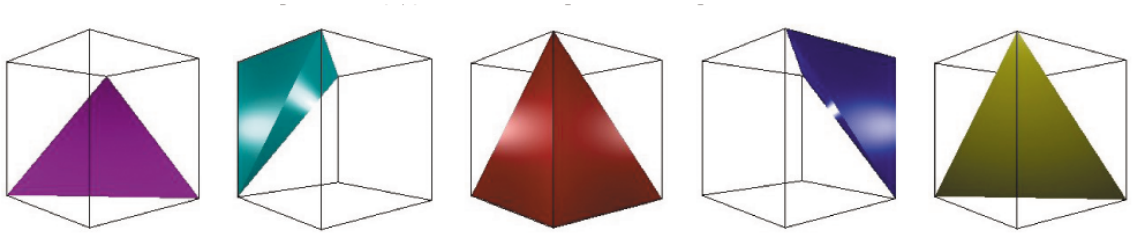

Figure 2.6: Five tetrahedra that make up each cell[2]

Figure 2.7 shows a circle that was not able to be lined up exactly with the cartesian mesh. Cuts were made (shown in red with the original outline shown in dark green) to represent the circle with slices through each element. This simple 2-D demonstration helps to illustrate how the tetrahedra work in 3-D to define the boundaries of complicated shapes. For this circle, the slices line up almost exactly with the original border, but computations can be performed much faster on this mesh.

In this figure, the lighter green/pink elements represent what are called interface elements. These are the elements where a cut has been made. As they contain both internal and external space, they may contain particles and internal surface volume.

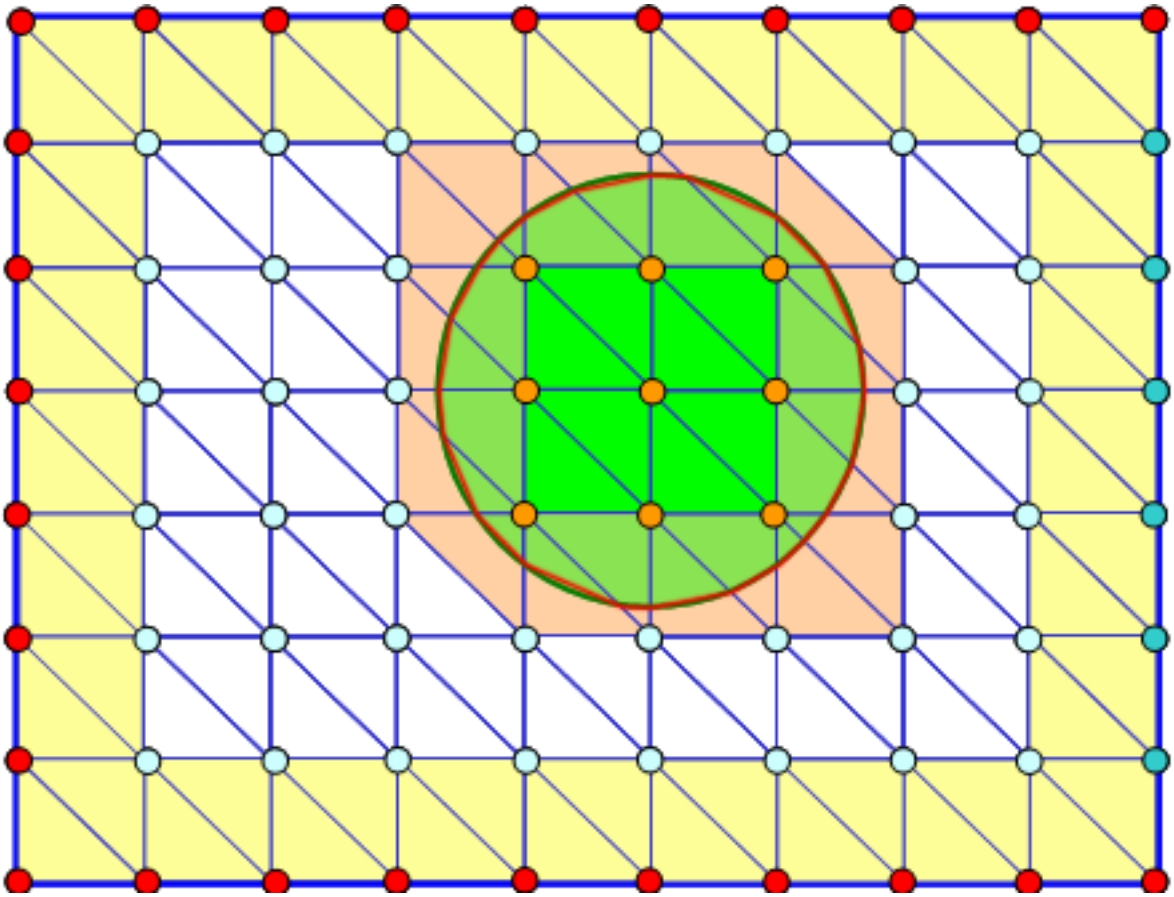

Figure 2.7: Sample grid overlay with interface cuts[3]

2.3.3 Charging Module

Surface charging is handled as a module that is incorporated into the DRACO code. The charge flux onto each node per timestep is saved and then a preset amount of time is simulated using that saved charge flux. This process can simulate large amounts of time quickly, but does not recompute the electric field, so it must not be set too high. After a simulated charge run, the PIC simulation is run for a set number of timesteps in order to recalibrate the electric field to the new surface charge. The charge flux is recalculated and the process runs again.

Several values must be specified in the Coliseum input files. The material file requires two new columns, permittivity, measured in Fm^{-1} and conductivity, measured in Sm^{-1}. These values are used in the storage of distribution of charge in the surface material. The component file requires a new column, thickness, measured in m. This is a measure of the surface thickness for each component. If the thickness is set to 0, then it is assumed there is no coating on the component, and all current goes directly to the interior of the spacecraft.

This process is controlled by several numbers specified in the *coliseum.in* file. The first is the coliseum variable, nt_charging. This is set via a coliseum SET statement and can be either -1 to turn charging off or a positive integer which represents the interval of timesteps between charging runs. So a user would specify SET nt_charging N to have coliseum perform a charging calculation every N timesteps.

Next, the user uses the DRACO_INIT_CHARGING command to specify all of the charging parameters. The usage of the command is:

DRACO_INIT_CHARGING *iterations dt_multiplier nt_output sub_cycles mode ground_potential capacitance filename*

Iterations is the number of iterations to simulate in this calculation. An iteration value, N, would run N timesteps of charging with the current particle flux.

The *dt_multiplier* parameter is a measure of how much to multiply *dt* by for each iteration. For example, if the PIC timestep was 10^{-11} seconds as is often the case in full PIC simulations, multiplier of a few thousand might be used since the overall charge will have changed little in 10^{-11} seconds.

The *nt_output* parameter is a measure of how often to output surface charging data to a Tecplot format file. This parameter can be either positive or negative. A positive value of N will output data every N iterations of the current charging run. A negative value does not actually imply 'negative', but instead means that the value applies to the PIC timestep and not the local iteration. It therefore will output data ever N PIC timesteps, at the end of the charging run. If the runs are generally short, but frequent, then a negative value would be used, whereas if the runs were long and far apart, then a positive number may be used. If a negative value is used, it must be a multiple of the *nt_charging* value in order to be called. For example, if *nt_charging* is set to 3, and and *nt_output* is set to -5 then although

the values of 5 and 10 line up with the every 5 PIC iterations specified, the charging code is not run at those iterations since 5 and 10 are not divisible by 3. The first output would therefore be at PIC timestep 15. A value of 0 can also be used to simply mean output once every charging run. This is equivalent to setting nt_output equal to $-nt\_charging$

The sub_cycles parameter is a measure of how many iterations the movement of charge over the surface are used for each overall charging iteration. When a geometry has a large number of small cells and a finite conductivity, charge will conduct over the surface. If sub_cycles is set to N, then for each iteration the charge will be able to propagate N cells away from its original location. This is because each sub cycle, the internal electric field is computed and the charge can be moved between neighboring elements. Since only neighboring elements are considered, it will take N sub cycles to propagate N elements away. The solving of the field and propagation of charge is one of the more computationally intensive aspects of the charging code so this number should not be increased higher than need be.

The *mode* value is a way to change the algorithms used for the charging routine. There are currently only two *modes* available to choose from. Setting the *mode* to 0 will enable a full PIC simulation where electrons and ions are both simulated as particles. Setting the mode to 1 will employ the Boltzmann electron approximation to calculate electron flux and model only ions as particles. In the future as new algorithms are added, they will be controlled here.

The *ground_potential* is the initial charge to place on the surface. In the *component.txt* file, a potential on each component can be set. As the ground potential is shared by all components while the potential specified in the component file is component specific, the difference between the component potential and the ground potential is considered to be an initial surface charge. So if a *ground_potential* of G and a component potential of C are specified, then the component will have a total charge of C, where the internal spacecraft ground contributes G and the surface contributes $C - G$. In most cases, the component potential should simply be set to the *ground_potential*, however if a simulated surface charge is desirable, this is a simple way to add one. More advanced methods of setting initial charge values are discussed in Section 3.5.2.

The internal ground, is charged via the specified *capacitance* here. It is often difficult to obtain a correct capacitance for an arbitrarily shaped object, so an approximate value is often used, such as that of a sphere. In future versions, an immersed finite element solver will be incorporated which will solve the potential inside the object and remove the need for a capacitance value.

Initial values can be loaded using the $filename$ parameter. Values for internal driving voltages, such as the gradient on a solar panel, and initial charge in the surface can be loaded at every point on the spacecraft. The format used is the same Tecplot format used when saving output data, so this provides a convenient way not only to set initial conditions, but to resume

an old simulation as well. If no *filename* is specified, all values are set to 0.

Chapter 3

Algorithms

3.1 Surface Detection

The first step for a differential charging calculation is to determine where on the surface to add charge. Since this code uses a full PIC particle method and charge is transferred to the surface via particle impacts, this becomes a question of where the particles impact the surface.

This process is described as follows, and is also shown in a flowchart in Figure 3.1. If the particle is detected in an interface or boundary cell, it is immediately known where the particle impacted. If a particle is detected in an internal cell, it is backtracked along its velocity vector until it is in either an interface, or boundary cell. Once it is in one of these two cell types, the element that the particle passed through can be easily determined based on which way the elements are facing. Once the element of impact has been

determined, that charge can be applied to it as discussed in Section 3.4.

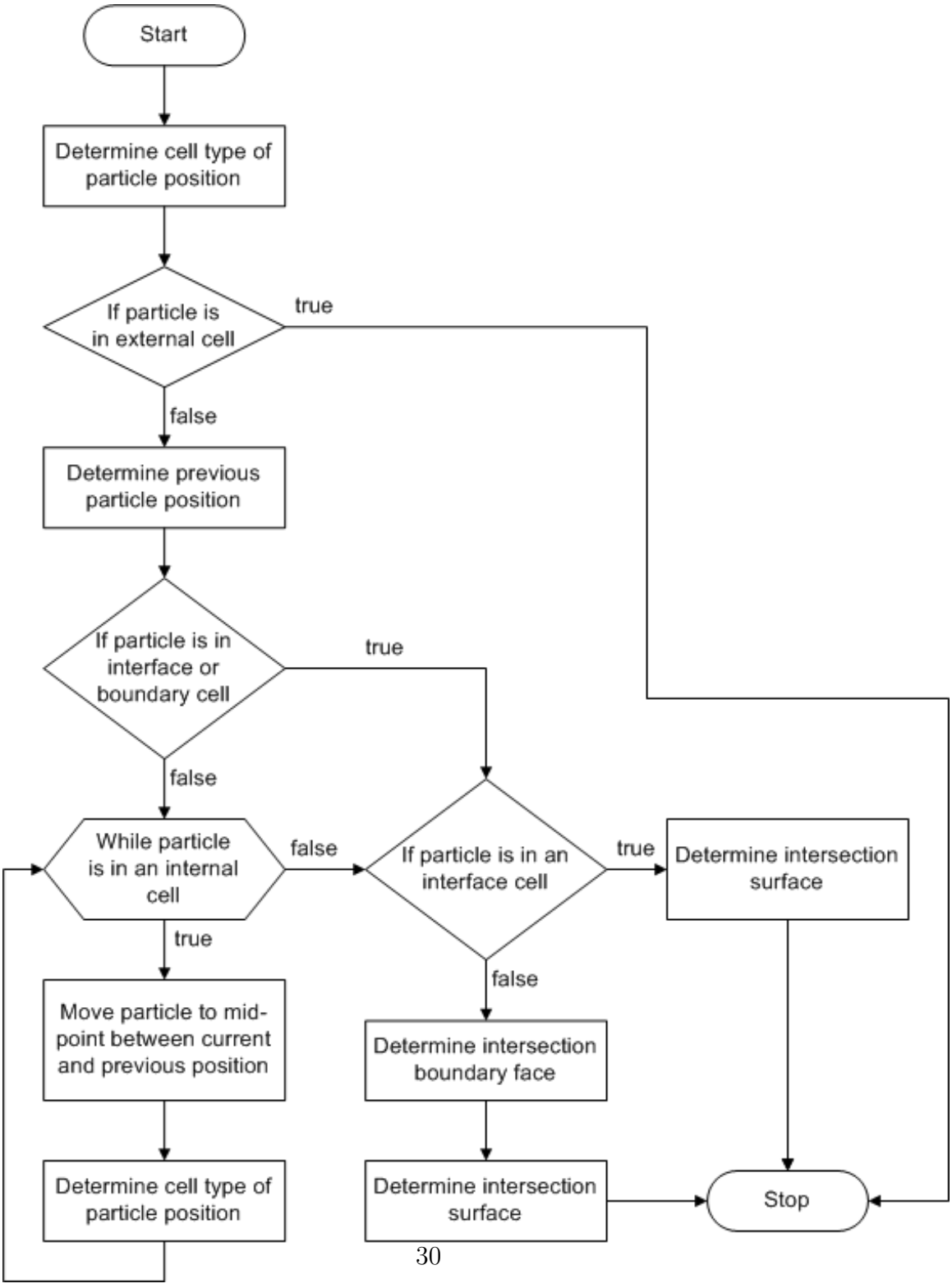

Figure 3.1: Flowchart representing the algorithm for surface element detection upon particle impact

3.2 Physical Model

The following physical model was used when designing the code and associated algorithms used in this thesis

- Ions and electrons can both be modeled as particles, or alternatively, the electrons can be modeled as a fluid using conservation and continuity equations. The particles will move according to the local electric field.
- Particle collisions will be modeled.
- Particle that impact the surface can reflect in a specular or diffuse fashion, or they can be absorbed by the surface. All absorbed particles will impart their charge into the surface at the location of impact.
- Charge is able to flow through the surface material based on the chosen material conductivity and the electric field inside the surface material.
- Each surface element is two dimensional allowing it to be modeled as a conductive plate with a dielectric material on one side. This simplifies down to a generic parallel plate capacitor.
- Surface elements can have a potential bias, such as in a solar array.
- Charge that flows through the surface material into the interior of the spacecraft can be either added to the local ground potential or discarded.

- All interior elements of the spacecraft are electrically connected.
- Each component of the spacecraft can have a different surface material and thickness.
- Components with no surface applied are considered conductive and connected directly to the local spacecraft ground.
- The ground potential of the spacecraft is calculated based on a specified capacitance value.
- The electric field in the plasma environment will be resolved periodically to update the current collection values for the spacecraft.

3.3 Current Collection

This module offers two methods of particle tracking: a full PIC method which models both ions and electrons, and a Boltzmann electron approximation, which models only ions as particles and uses an approximation for the electron density. The time complexity involved in modeling electrons vs. ions is discussed in Section 3.5.

Before the module can be trusted for complex charging calculations, current collection must be validated. Current collection is often times the major source of error in charging analyses. Therefore, to test these two methods, a test case was run immersing a sphere into a uniform, stationary, $10eV$ ambient plasma (Fig. 3.2, Table 3.1) and the current to the sphere was measured.

ion density (m^{-3})	3×10^{12}
electron density (m^{-3})	3×10^{12}
temperature (K)	750
ion	$O+$

Table 3.1: Plasma parameters for spherical probe test

As Prokopenko and Laframboise have shown[49], current density to a sphere can be calculated as

$$j = j_0(1 - \frac{qV_s}{kT}) \tag{3.1}$$

for the attracted species and

$$j = j_0 \left(exp \left(\frac{-qV_s}{kT} \right) \right) \tag{3.2}$$

for the repelled species, where j_0 is the ambient current density, given by

$$j_0 = \frac{qn\bar{c}}{4} \tag{3.3}$$

with $\bar{c}$ being the thermal velocity,

$$\bar{c} = \sqrt{\frac{kT}{m}} \tag{3.4}$$

This analytic result was used for comparison.

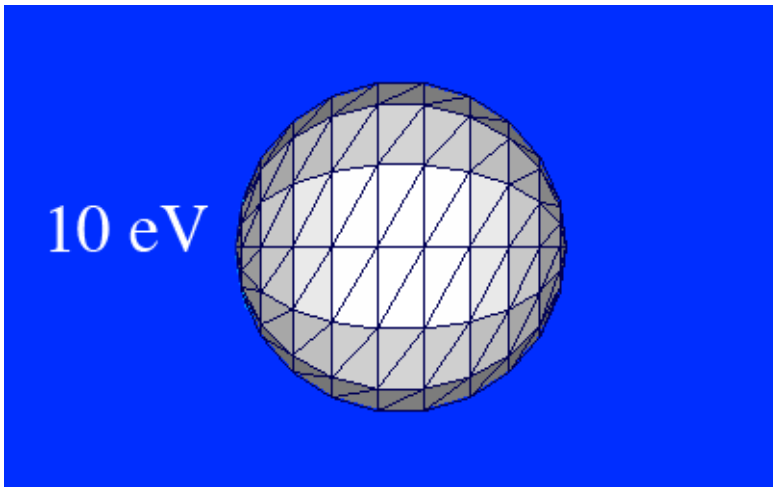

Figure 3.2: Initial setup for spherical probe in ambient plasma current collection test

3.3.1 Boltzmann Electron Approximation

The Boltzmann model, shown below in Equations 3.5 and 3.6, is a way to estimate electron density. The Boltzmann electron model approximates electron flux and avoids having to model electrons as particles.

$$n_e = n_{e\infty} exp\left(\frac{e\phi}{kT_e}\right) \tag{3.5}$$

$$q = -n_e v_{th} dt \tag{3.6}$$

The problem with the Boltzmann approximation, as shown in Figure 3.3 is that it is only accurate for negative or low potentials. The simulated current tends to fluctuate up and down due to random variance in particle flux. This is shown in the error bars in the figure and is generally small compared to the overall value.

For the sphere test case, the approximation started to break away almost immediately once a positive potential was applied to the sphere. The ion current did not overtake the electron current, however, until the sphere had $8V$ applied to it. Since a current dominated by electrons will lower the potential on the sphere, the approximation will become more accurate as the simulation progresses and will eventually arrive at the correct potential for the surface of the sphere. This means that the Boltzmann model can still be used for positive potentials as long as the current remains electron dominant,

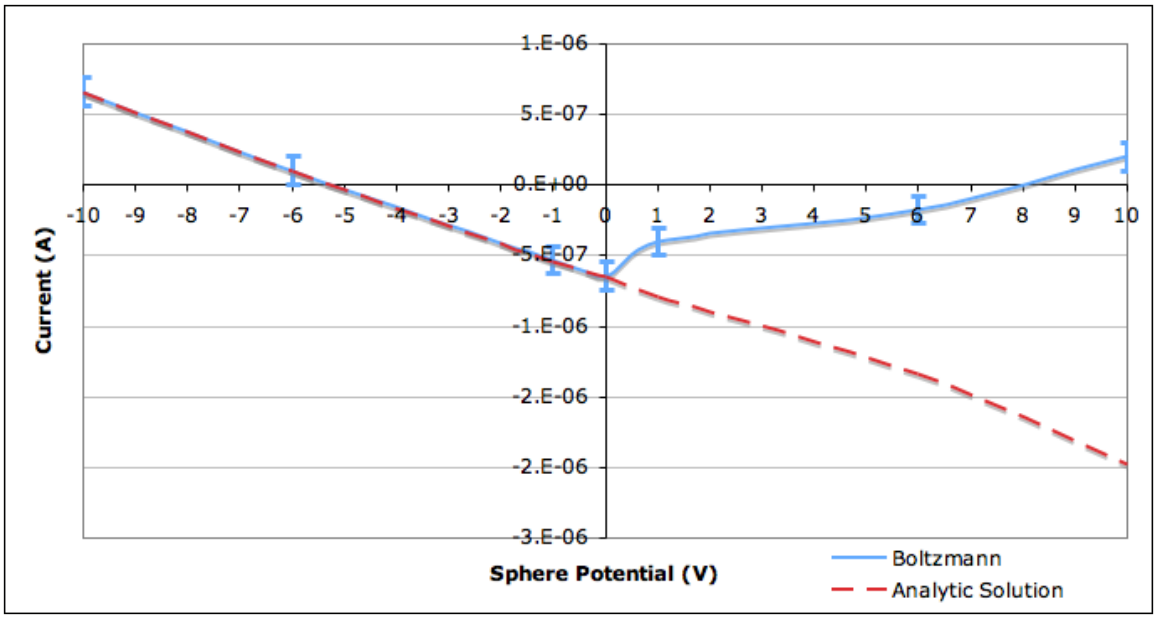

Figure 3.3: Current collection on sphere from Boltzmann electron approximation compared to analytical results

and will therefore end with a negative potential at steady state.

It is possible to take advantage of this and simulate certain cases that have high initial potentials. In many cases the ambient plasma is quasi-neutral. Since electrons have a higher thermal velocityand are therefore more likely to impact the surfacemost surfaces will tend to have a slight negative potential. An initial surface charge map can be loaded to simulate a potential of near $0V$. This will not change the internal potential of the object, it simply assumes that if a full PIC charging simulation were run, it would at some point charge the surface to near $0V$ and skips that process by starting with that amount of charge already accumulated. The Boltzmann case can then

be run to progress towards the correct potential map of the surface. In some cases, however, the assumption of a negative, or low positive final potential cannot be made and a a full PIC model must be used.

3.3.2 Full PIC

The full PIC mode models both ions and electrons. Because electrons have such a high thermal velocity, a small cell size or timestep must be used to ensure accurate particle tracking. Lowering the timestep can be problematic since a long simulation time will be required in order for the ions to reach a steady state. One way to mitigate this problem is to run the ions separately. The ions can be modeled with background electrons, instead of particles, until the field reaches a steady state. The particle positions and velocities can be saved at this point and then loaded into a full PIC simulation. This approach was used in the spacecraft based simulations presented in this paper.

If a smaller domain size is preferable to a low timestep, that can be accomplished in two ways. The first, is to simply shrink the domain by a scale factor so that the cell size is on the order of millimeters. The second is to simulate only the domain close to the surface as a full PIC and to calculate the overall plume and plasma contours with less stringent size requirements. In this case there is no reason not to have a small domain, so a sphere with radius $1.5mm$ was used and a domain size of $3cm$ on a side. The current collection comparison is shown in Figure 3.4.

This shows almost exact agreement between the simulated results and the analytical results for the positive voltages that the Boltzmann model could not correctly predict. The accuracy of the full PIC current collection model is accurate enough to justify simulating more complicated geometries, that do not have analytical solutions, with confidence.

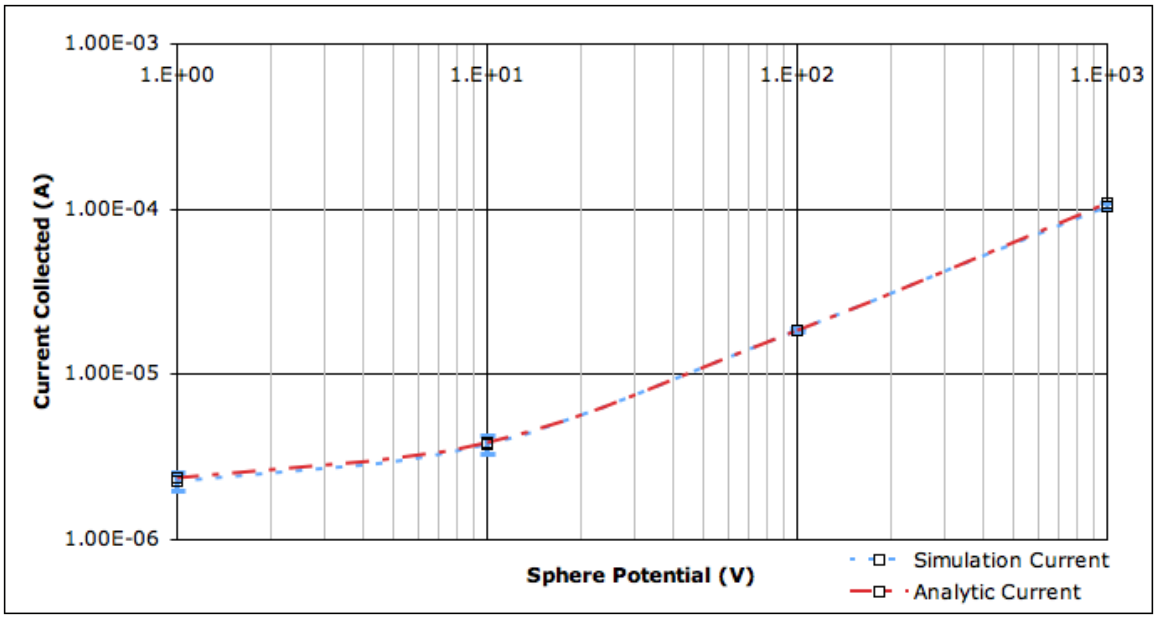

(a) Current collection for positive sphere potentials

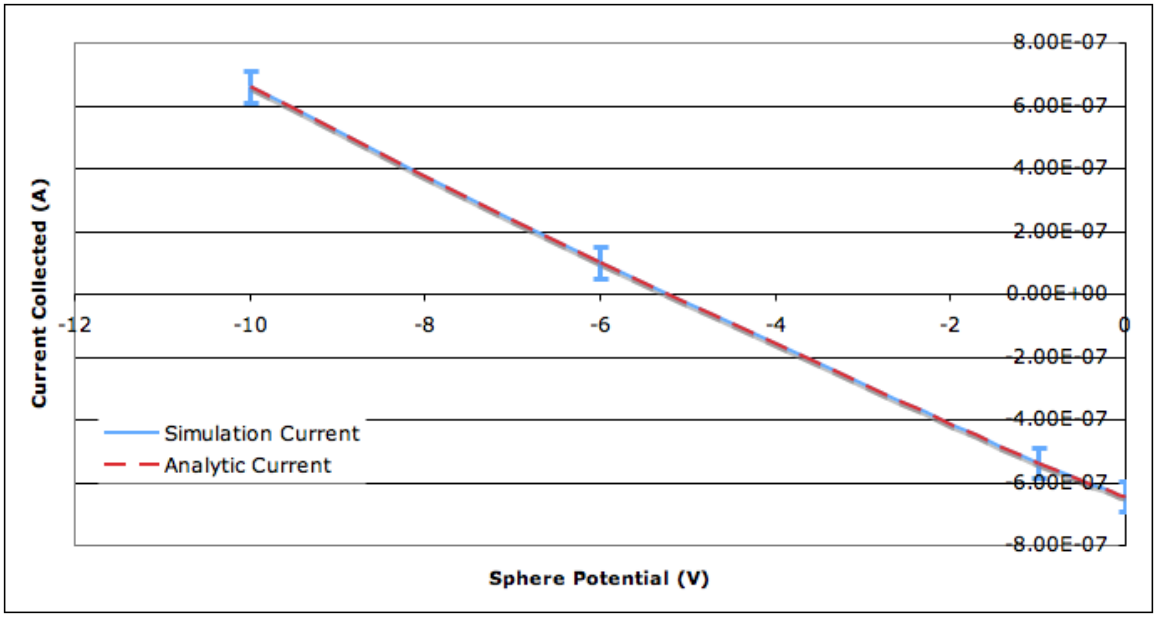

(b) Current collection for negative sphere potentials

Figure 3.4: Current collection on sphere from full PIC simulation compared to analytical results

3.4 Charge Movement

Since the material of the surface is uniform and has finite thickness, charge can propagate through the surface in any direction. This is governed by the local electric field inside the material. The movement is broken down into two components: one through the material into the interior of the spacecraft, and one across the material into neighboring elements. This is shown in Figure 3.5.

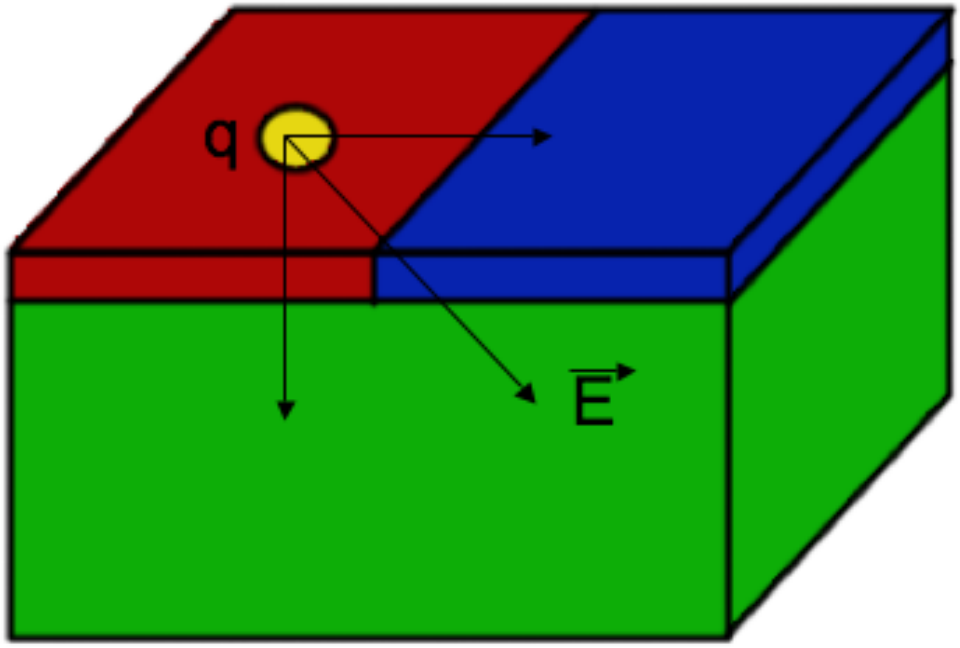

Figure 3.5: Two components of charge movement governed by local electric field

3.4.1 Conduction to Ground

If the surface has a finite conductivity, then some charge will be conducted through the surface into the interior of the spacecraft. If the conductivity is high enough then all the charge will flow through the surface resulting in a uniform spacecraft charge as opposed to a potential difference between the surface and interior of he spacecraft. This must be taken into account before charge is accumulated on the surface.

Charge that flows through the surface in this way is added to the spacecraft ground potential via the capacitance given in the coliseum.in file. The interior of the spacecraft is assumed to be conductive, so that only one ground value and capacitance value is needed for the entire spacecraft.

Current density j is a function of electric field E and conductivity σ.

$$j = \sigma E \tag{3.7}$$

Using displacement D and charge density ρ, along with the area of the element A, electric field can be solved as a function of charge q.

$$\rho = \frac{q}{A} = D = \epsilon E \tag{3.8}$$

$$E = \frac{q}{A\epsilon} \tag{3.9}$$

The total electric field inside the material is the difference between the

two opposing fields due to the charge on the interior E_{is} and surface E_{si} of the spacecraft.

$$E_s = E_{is} - E_{si} \tag{3.10}$$

A function of potential and surface thickness is also incorporated to allow for the inclusion of the interior potential, ϕ_i to be used.

$$E = \frac{\phi}{t} \tag{3.11}$$

$$E_s = \frac{\phi_i}{t} - \frac{q_s}{A\epsilon} \tag{3.12}$$

The current density through the surface, from Equation 3.7 can then be multiplied by the element area to gain the overall current through the surface.

$$i_s = j_s A = \sigma \left(\frac{A\phi_i}{t} - \frac{q_s}{\epsilon} \right) \tag{3.13}$$

3.4.2 Conduction Around Surface

In addition to conduction through the surface, charge can also propagate along the surface. This is handled here in several steps.

First, the electric field is solved between all neighboring nodes, a and b on the surface separated by a distance, dx by the equation

$$E_{ab} = -\frac{\phi_a - \phi_b}{dx} \tag{3.14}$$

Since each element is flat, and only the field between adjacent nodes is considered, this can be considered a 1-D problem in the local area of interest regardless of the actual geometry. Current density can therefore be calculated per unit length by multiplying the electric field by the material conductivity

$$j_{ab} = \sigma E_{ab} \tag{3.15}$$

Current density can then be multiplied by a cross sectional distance to get a current between nodes a and b.

$$i_{ab} = j_{ab} dy \tag{3.16}$$

A cross sectional distance is not an immediately obvious quantity to obtain, since all of the elements are triangular. In this case, the area surrounding the node is assumed to be 1/3 of the area of each triangular element that includes the node allowing for the square root of that area to be a reasonable

choice for a cross sectional distance. Given that the material is uniform, this is a reasonable approximation as long as the surface elements are roughly the same size. If one element is much larger than another then a skewed distance calculation may result.

Finally, the current between each set of the n neighboring nodes is multiplied by the timestep and added up to obtain a change in charge on each node.

$$dq_a = \Sigma_0^n i_{na} dt \tag{3.17}$$

3.4.3 Conversion to Potential

Charge that is conducted through the surface to the interior of the spacecraft is added to the overall internal potential, or ground potential, of the spacecraft.

$$dq_i = Cd\phi_i \tag{3.18}$$

where C is the capacitance of the spacecraft. In order to employ this, the capacitance must be known. This value does not, however, have to be extremely accurate. As shown in Equation 3.18, the relationship between charge and potential is linear, varying in slope proportional to capacitance. Combining this with the fact that the steady state potential map is essentially a balance between the surface potential and ambient potential, the capacitance of the spacecraft will not affect the overall potential map in the steady state. The only effect that a change in capacitance will bring about is a difference in the time rate of change of the potential map of the surface. If the simulation is left to run until a steady state is reached, and the intermediate values are not important, then the spacecraft capacitance can be an approximate value, such as that of a similarly sized sphere, and will yield correct results.

Alternatively, if a capacitance of 0 is specified, then all charge conducted into the interior of the spacecraft will be simply discarded. This can be used to simulate an electron gun, or a conducting gradient out of the scope of the

simulation, or some other method of removing charge. Both of these capacitance choices are demonstrated in the plume impingement case, described in Section 4.1.

The total charge on and around the surface is converted to potential based on the values of the internal potential, ϕ_i, and the surface charge, element area, and thickness and permittivity of the surface material.

$$\phi = \phi_i + \frac{q_s t}{A\epsilon} \tag{3.19}$$

As shown in Figure 3.6, the internal potential is equal to the ground potential plus any applied voltage difference, such as in a solar array. The final potential as seen by the ambient plasma is therefore affected by three different sources: the ground voltage, the applied voltage, and the charge stored in the surface.

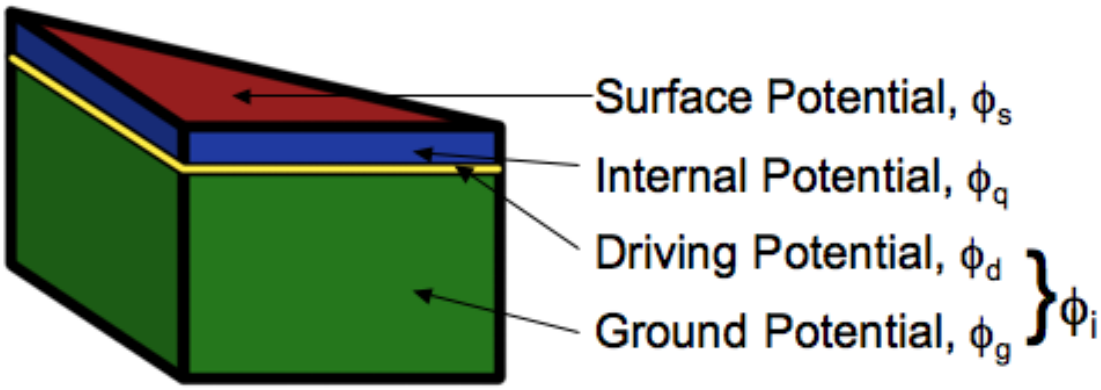

Figure 3.6: Model for a sample element with a driving voltage applied

3.5 Time Management

Electrons have a much higher thermal velocity than ions, due to their lower mass. This is shown in Equation 3.20. Ion masses tend to be on the order of 10^5 times that of electron masses, resulting in an electron thermal velocity of over 300 times that of the ions.

$$\frac{v_{the}}{v_{thi}} = \sqrt{\frac{m_i}{m_e}} \tag{3.20}$$

For accurate particle tracking, DRACO requires that particles not move more than one cell per timestep so that the particle velocity can be readjusted based on each cell's local electric field. Therefore, electrons require a much smaller cell size or timestep if they are to be modeled as particles since they move so much faster.

If computation time is not a concern, the cell size can simply be shrunk, or the timestep lowered to ensure that particles move, on average, less than one cell length. DRACO has a dynamic timestep capability which allows the timestep to be computed based on average particle velocity. This number can be set to a number around 0.75, which would mean that the average particle would move 0.75 cell lengths in that timestep.

In order to lower the cell size without increasing computation time, the overall number of cells must stay the same. That requires a smaller domain. This can be accomplished by modeling only a section of the spacecraft instead of the entire spacecraft. This can be accomplished by running a fluid

electron model for the overall plasma environment, and then running a full PIC simulation for the area of interest. This technique was used in Section 4.3.

Another method is to use multiple grid sizes. The overall domain can use a coarse grid, while the area of interest can use a fine grid. This method has been newly incorporated into DRACO and is discussed at length in Ref. [50].

If CPU time is important and domain size cannot be lessened, then it must be evaluated whether it is worth the extra computation to compute electrons as particles.

3.5.1 Timestep Multiplier

As discussed in Section 2.3.3, the charging module has a dynamic timestep employed which allows for a variety of plasma environments to be simulated efficiently. The basic command usage in the coliseum.in file is

> DRACO_INIT_CHARGING *iterations dt_multiplier nt_output sub_cycles mode ground_potential capacitance filename*

The key parameters for time management are *iterations*, *dt_multiplier*, and *sub_cycles*, along with the coliseum variable *nt_charging*. This section describes some general guidelines for how to choose values for these parameters based on simulation conditions.

- In cases where all surfaces are non conductive, *sub_cycles* can be set to 0 since no conduction of current will take place. There is then no need for multiple iterations and *iterations* can be set to 1.

- The *nt_charging* parameter should be set such that the PIC simulation has time to respond to increased charges before another charging iteration is performed. The charging routine takes the number of particles hitting each element in the surface for the timestep immediately preceding the charging timestep and uses that set of numbers for input throughout that round of charging. If there is little difference in potential in each round of charging, then a small value can be used for *nt_charging*. If a large amount of potential change takes place,

however, a large value must be used in order to give the PIC time to update the field properly. If the field does not have time to respond to the new surface potential then inaccurate results for particle counts may result in the next charging round.

- In low density environments, such as GEO or interstellar space, a high *dt_multiplier* can be implemented. This allows even low density environments to impart a large number of particles on the surface during each iteration. Values on the order of 10^8 or higher are not uncommon for low density environments. Setting this value higher will result in a shorter simulation time to reach a steady state, but can also add noise. If, for example, one element gets five particles and a neighboring element gets only one, then a multiplier of 10^8 would result in 4×10^8 more particles hitting that first element than the second. Generally, these differences will even out given time, but if the value is set too high, and the *nt_charging* variable is set low, then large differentials may appear. This is shown in Figure 3.7. This setup was a uniform plasma, but the potential map is largely skewed because of the multiplier being high and *nt_charging* being low.

- Conversely, in a high density environment, such as plume impingement, a low *dt_multiplier* must be used. Values on the order of 1 were used for the plume impingement cases discussed in Section 4.1. Values much less than 1 can be used if necessary, in the case of extremely large densities.

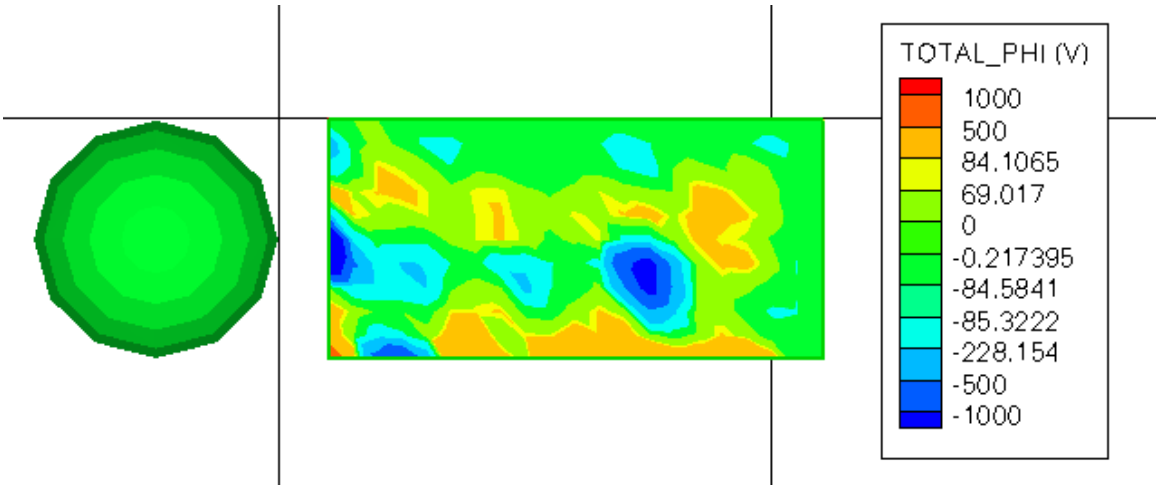

Figure 3.7: Simulation with large timestep multiplier resulting in large amount of noise

- The *sub_cycles* parameter should be assigned proportionally to the conductance of the outer surface, and the number of elements comprising the surface. This parameter controls how many elements the current may propagate through per iteration. Therefore, a large conductivity, or small number of elements lends towards a larger number of *sub_cycles*. Typically, a value of 25 is plenty unless there is an unusually large number of elements on the surface. If a larger value is necessary, it may be advantageous to simply consider the body conductive and remove the computation involved in charge propagation through a semiconductive surface.

3.5.2 Initial Loading Conditions

For full PIC simulations, the ion timestep is significantly larger than the ion electron timestep since the electrons have a much higher thermal velocity. If the ion timestep is used for the simulation, then the electrons will not be resolved correctly. If the electron timestep is used, then it will take a long simulation time for the ions to reach a steady solution. For this reason a form of subcycling is used for full PIC simulations.

Ions are run first, without electrons present, using the ion timestep. Additionally, a more simple solver such as the Boltzmann solver, can be used. This first run will use a fluid electron model to calculate the shape of the ion flow. Once this has been done, the particle positions and velocities are saved in a file.

Next, the simulation can resume by loading the particle file, but now the electrons are treated as particles, the electron timestep is used, and a more complex (DADI linear) solver is used. This allows for accurate particle tracking, but since the ions are already in their steady state formation, the correct number will impact the surface each timestep.

Initial charging conditions can also be loaded. The input format is the same as the output format so that an earlier output file can be used as an input in order to resume an old simulation. This file is also the means to load a driving potential, such as in the case of a solar array. The format is a standard Tecplot file, but must include every surface node for all zones. An example file is included in Appendix 5.2.

This file is not only used for initial setup, however, it can also be used to skip a large portion of simulation time, if values are chosen correctly. If the simulation is in a fairly uniform plasma, such as solar wind, or a GEO orbit, for example, then in most cases the floating potential of the spacecraft will be a slight negative value on the order of the electron temperature. This knowledge can be used to set input conditions that are an approximate guess of the final solution so that only small adjustments must be made by the PIC simulation, thus dramatically lowering execution time. If a gradient is to be used, the ground potential can be lowered initially to account for it.

In Section 4.2, for example the conductive, non gradient case shown in Figure 4.4(b) was run first to find the steady state floating potential. This value was found to be $-5.025V$. A $60V$ gradient was used for the rest of the cases. To account for the gradient, the ground was first lowered to $-30V$ to balance out input current. The ground voltage was then lowered by $-5.025V$ to account for the lowered floating potential. These inputs allowed for an approximate solution to be available from the start, resulting in short execution times.

This type of initial guess can be especially important when again considering the slow movement of ions. Even if the initial ion map is accurate, it will change throughout the simulation as the charging occurs, which can extend the overall computation time. Using intelligent inputs will help to counteract this effect.

Chapter 4

Modeling Test Cases and Results

4.1 Plume Impingement on Spherical Probe

The first example investigates surface charging induced by the impingement of an ion thruster plume on a spherical probe. The purpose of this case is to investigate the effect that different material configurations will have on the surface potential gradient of the probe.

This can be of great concern in space mission applications, since materials are often governed by several different factors such as heating and cooling properties, particle absorption, structural strength, etc. As some of these issues may take priority over surface charging concerns, it is important to understand how these different materials may behave in a space environment.

The simulation setup is shown in Figure 4.1. In this simulation, a composite sphere is placed in front of an ion thruster beam in a vacuum environment. The sphere material properties and dimensions, as well as the thruster parameters are listed in Table 4.1.

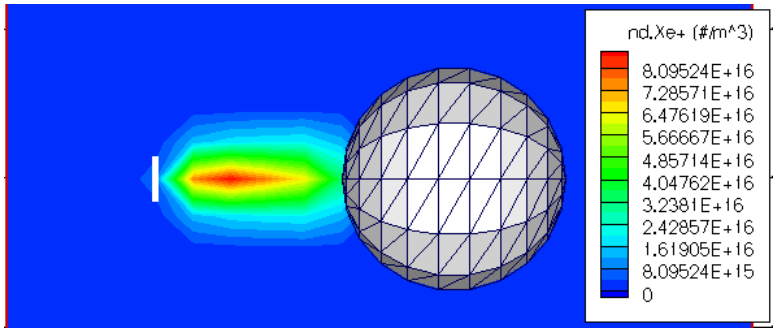

Figure 4.1: Simulation setup for a sphere under the impingement of ion thruster plume with the thruster plume number densities.

The sphere considered here consists of an interior sphere with a thin coating. Three different material compositions are presented. In the first two cases, the interior sphere is assumed to be a charge sink. This means that all charge that reaches the interior sphere is removed immediately. This mode can be used to model an electron gun, or a voltage gradient carrying charge elsewhere in the system.

The coating shell in the first case is non-conductive (e.g. glass) and in the second case is semi-conductive (e.g. silicon). In the third case, the charge sink is removed and the interior sphere is a conductor *not* connected to a ground. The coating is again semi-conductive.

Figure 4.2 compares the response in surface potential for each case. In

Sphere			
	Case 1	Case 2	Case 3
surface conductivity (Sm^{-1})	0	10^{-5}	10^{-5}
surface permittivity (Fm^{-1})	10^{-11}	10^{-9}	10^{-9}
surface thickness (mm)	1	1	1
initial potential (V)	0	0	0
interior sphere capacitance (pF)	N/A	N/A	0.168
interior sphere conductivity (Sm^{-1})	N/A	N/A	10^{11}
interior sphere	charge sink	charge sink	conductive body
sphere radius (mm)	1.5	1.5	1.5
distance from center of sphere to thruster (mm)	0.2	0.2	0.2
Thruster			
thruster exit radius (mm)	0.025	0.025	0.025
mass flow rate (kgs^{-1})	1.089×10^{-6}	1.089×10^{-6}	1.089×10^{-6}
exit temperature (K)	19161	19161	19161
exit velocity (ms^{-1})	11604	11604	11604
beam divergence (^{o})	10	10	10
ion	$Xe+$	$Xe+$	$Xe+$

Table 4.1: Parameters for sphere under plume impingement test.

this figure, the view angle is a 45 degree rotation with respect to the thruster firing direction to show both sides of the sphere.

When the surface coating is non-conductive, as in the first case, the result shows that a large amount of differential charging is developed between the side facing the thruster and the side opposite the thruster. The charging is due to non-uniform charge deposition on surface by the plume. This case is of the greatest concern, as it can lead to arcing across the surface.

The second case shows the effect of a small amount of conductivity in the surface. The charge is then allowed to flow through and around the surface

material. The potential gradient reaches slightly further around the sphere than the first case due to the flow of current along the surface, but a far greater amount of charge flows through the surface into the interior. This is expected since the material is uniform and the thickness is small compared to the surface area of the sphere.

This flow through the surface can, as shown, greatly reduce the potential gradient across the surface of the sphere. Because the conductivity was not sufficiently high enough to lead to a uniform surface, there is a potential gradient similarly shaped to case one. However, unlike case one, the magnitude is lowered to a point where the potential gradient is no longer a concern. Thus, if there is a way to conduct away internal charge (a charge sink), then a small amount of conductivity in the surface can lead to a greatly reduced surface potential gradient.

The third case shows an example of the same probe, except that a charge sink is no longer available and has been replaced by a conducting body. The surface still has the low conductivity seen in case two. In this setup, the potential again flows into the interior of the spacecraft, but now is redistributed by the conductive interior. Since the surface can have charge flow to or from the interior, this redistributed charge is then reabsorbed into the surface. This eventually creates a uniform surface potential as shown in Figure 4.2(c).

In this case since the charge cannot be removed, it must be stored in the surface. This can eventually lead to high potentials; however if the surface

can be made uniform, there will be no chance for arcing since the potentials will all be low with respect to other points on the spacecraft.

What this last case essentially shows, is that when a surface cannot be totally conductive due to material constraints, a small amount of conductivity may suffice as long as a conductive interior layer is available to redistribute the charge absorbed by the surface. This setup can essentially mimic a conductive outer layer, allowing a surface such as silicon to function as well as aluminum in terms of charge redistribution on the surface of the spacecraft.

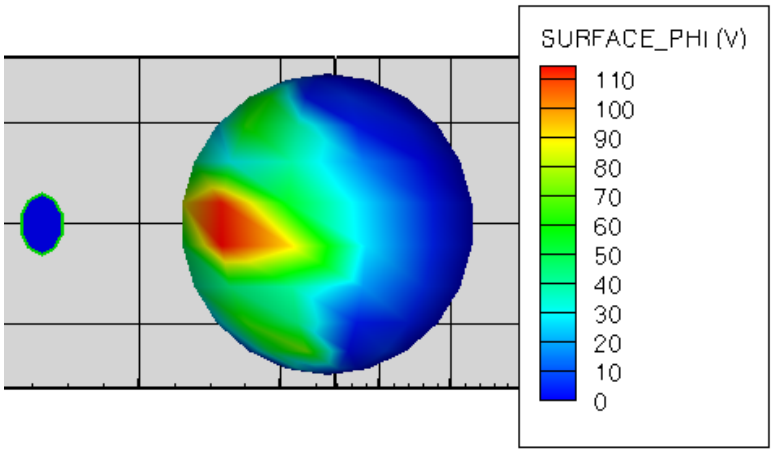

(a) All charge movement turned off

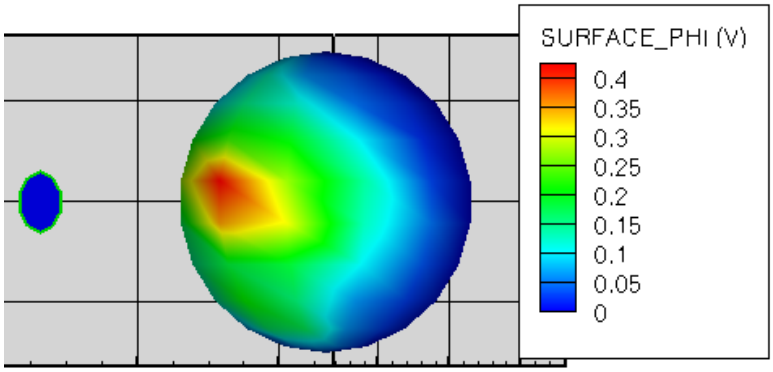

(b) Charge movement on with interior charge sink

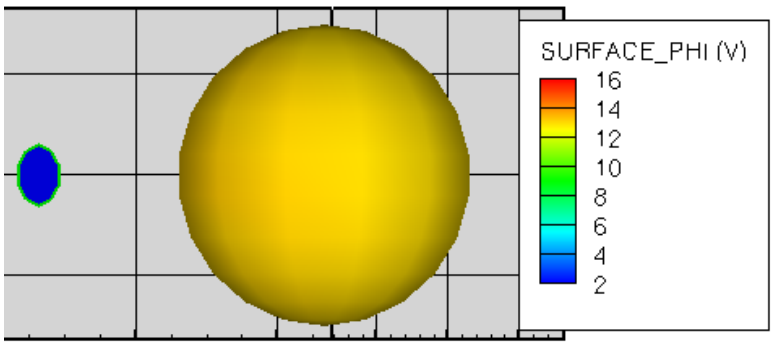

(c) Charge movement on with conductive interior

Figure 4.2: A spherical probe exposed to an ion thruster plume

4.2 Spacecraft in Solar Wind

Next, a combination of structures of different materials immersed in a plasma is considered. The structure considered is a sphere with a thin panel, as shown in Figure 4.3. It is assumed that the panel may have an internal potential difference of 60 Volts covered by a surface coating between the two ends of the panel. The sphere is electrically connected to the negative ground of the panel. Each case has different material compositions.

The plasma environment considered is similar to that of the solar wind at $1AU$, drifting directly into the upper surface of the panel. The plasma parameters are shown in Table 4.2. The only current sources considered here are the ambient electrons and ions. Other current sources, such as photoelectrons, are not considered.

The parameters for the spacecraft setup are listed in Table 4.4. Full particle PIC is used for this simulation.

n_{e1} (cm^{-3})	3.5
T_{e1} $(eV$ $)$	40
n_{i1} (cm^{-3})	3.5
T_{i1} $(\ eV\ )$	10
V_d (kms^{-1})	400

Table 4.2: Parameters for ambient plasma environment

Two conductive cases were run first, to ensure correct conduction of current around the spacecraft. The first case, shown in Figure 4.4(b), shows the spacecraft with all conductive surfaces and no interior driving voltages

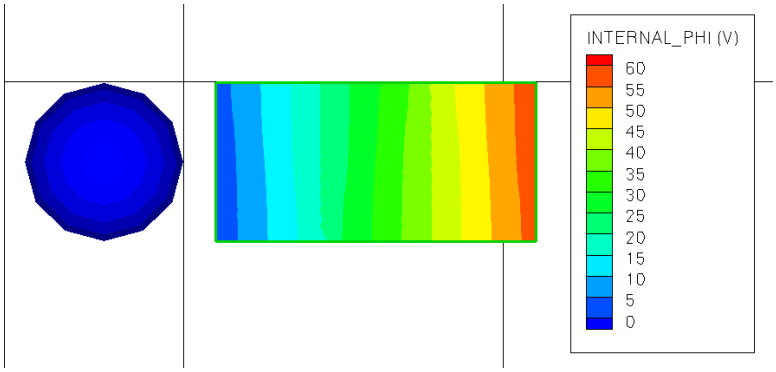

Figure 4.3: Spacecraft geometry and initial driving potential map

Dielectric Elements	
conductivity (Sm^{-1})	10^{-10}
permittivity (Fm^{-1})	10^{-11}
surface thickness (mm)	2.5
Conductive Elements	
conductivity (Sm^{-1})	10^{11}
body capacitance (F)	27.78×10^{-6}
Semi-Conductive Elements	
conductivity (Sm^{-1})	10^{-5}
permittivity (Fm^{-1})	10^{-9}
surface thickness (mm)	2.5
Geometry	
sphere radius (m)	0.25
panel length (m)	1
panel width (m)	0.5
panel thickness (m)	0.05
distance between sphere and panel (m)	0.10

Table 4.3: Parameters for components of spacecraft

	Case 1	Case 2	Case 3	Case 4
panel front surface	conductive	conductive	dielectric	dielectric
panel back surface	conductive	conductive	dielectric	conductive
panel potential gradient	not applied	applied	applied	applied
sphere surface	conductive	conductive	dielectric	conductive

Table 4.4: Spacecraft component materials

applied. The spacecraft reaches a steady, uniform potential of $-5.025V$. At steady state a net current of 0 must be maintained, meaning that the floating potential for this surface is right around $-5V$.

The second case, shown in Figure 4.4(c), shows a fully conductive spacecraft, as in the first case, but this time the $60V$ driving voltage was reapplied across the panel. Since the voltage gradient is applied to the local spacecraft ground, and a current balance must be attained for steady state, the ground voltage lowered to accommodate the driving gradient. The final gradient ranged from $-35V$ to $+25V$, for a range of $60V$. This is in perfect agreement with the first case, which had a floating potential for the spacecraft of around $-5V$. $30V$ to the left of -5 and $30V$ to the right of -5 leads to a net current balance of 0.

A dielectric case was then run, where every surface was treated as nonconductive and no charge was allowed to move. This is shown in Figure 4.4(d). This case also had the initial driving voltage applied to the solar panel, but it does not show up in the steady solution. This is because the charge is not allowed to move on the surface, so the elements of the surface are essentially

independent, and will each charge up to the point of equilibrium with the environment. An element with a driving potential of $25V$ for example, will simply accrue -30 worth of charge in the surface to balance it out at the floating potential of $-5V$. For this reason, the entire panel ends up at around $-5V$ regardless of the interior gradient applied. There is some noise in this plot which is explained by the parameters of the plasma. Solar wind is a relatively low density plasma, meaning that relatively few particles hit the surface on any given timestep. For this reason, a large timestep multiplier must be used in order to complete the simulation in a reasonable amount of time. For this case, a multiplier of $1e6$ was used and the simulation was run for about twenty four hours. The noise results from the fact that some elements are bound to get a few more particles than others, and with a multiplier as high as this, those differences in particle counts are greatly magnified. Since these plots are all snapshots, the current noise is shown in the plot. If a time average were taken, then the noise would cancel out and a uniform plot would result. Further discussions into timestep management are available in Section 3.5. This case essentially shows that the internal ground potential, as well as any applied voltages, will be unimportant if a nonconductive surface is applied to the spacecraft. While this may seem attractive, Section 4.1 shows that a nonconductive surface can also lead to large differentials in potential across the surface. These effects must be taken into account when designing a spacecraft.

Next, a combination case with a conductive spacecraft body and panel

backing, and a dielectric coverglass on the solar panel, was run. These results are shown in Figure 4.4(e). As expected, the conductive elements reach a uniform voltage and the dielectric glass cancels out the applied gradient and reaches a uniform, if noisy, surface potential. This case illustrates that conductive and dielectric elements can be used in conjunction with each other and both reach the same resultant floating potential. It also illustrates that conductive elements will essentially filter out any noise in the particle flux by redistributing charge evenly over the conductive surfaces.

Finally, a test case with a semiconductive panel surface was run. This case shows a conductive sphere and panel backing, but the upper panel surface (coverglass) is neither conductive nor nonconductive, it has a small amount of conductivity. As Figure 4.4(f) shows, the driving potential gradient still shows up in the resulting potential, but to a lesser extent. The overall range of the gradient is decreased by $12V$. This is because the surface has a finite thickness and it takes a finite time for charge to flow through the surface. Because of this there will always be some charge in the surface. Since the number of particles that reach each element is related to the potential seen by the gradient, low potential areas will have more ions in the surface and high potential elements will have more electrons in the surface. This will act to blunt the effect of the gradient, such as in the dielectric case. The difference from the dielectric case, is that the charge will not sit in the surface forever, it will eventually conduct into the interior of the spacecraft and to the local ground. The rate at which particles are absorbed vs. the rate at which they

conduct through the surface controls the effect of the potential gradient on the surface.

At one extreme, the fully conductive case shows all the charge flowing to the ground and not storing in the surface at all. At the other extreme, the dielectric case shows all the charge storing in the surface and none reaching the ground. This semiconductive case shows a middle ground where the charge is stored in the surface for a time, but eventually conducts to the local ground and only somewhat masks the internal gradient.

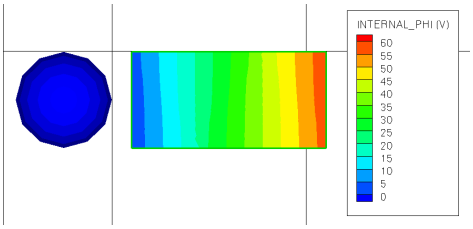

(a) Initial setup.

(b) All conductive surface elements with driving potential gradient removed.

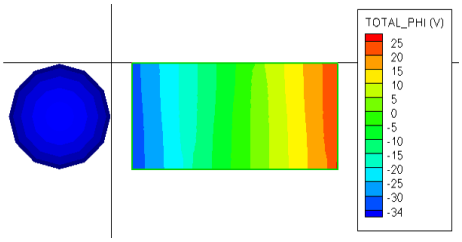

(c) All conductive surface elements.

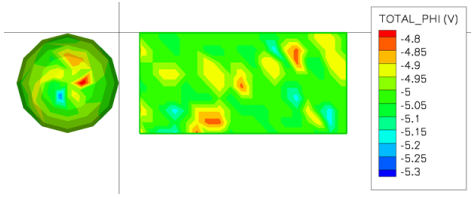

(d) All dielectric surface elements.

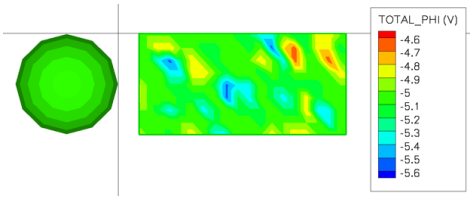

(e) Conducting sphere with dielectric cover glass on panel.

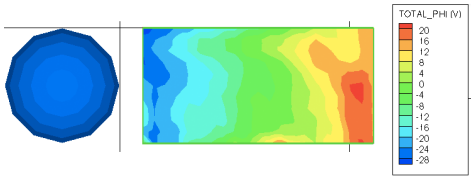

(f) Conducting sphere with semiconductive cover glass on panel.

Figure 4.4: Surface potential of a combination structure in a plasma similar to solar wind.

4.3 Panel in Thruster Plume

The final test case performed involved a spacecraft with a thruster plume. This simulation used a spacecraft model based on the DAWN[51] spacecraft. The spacecraft includes three NSTAR ion thrusters. The original plume simulation, in this case, was run first on a parallel system. The different subdomains used in the parallel setup are shown in Figure 4.5. The overall plume (particle positions, velocities, and charges) was then saved and imported into a DRACO charging routine. The parameters for the plume are shown in Table 4.5. Further information on the plume simulation is available in Reference [43].

While the plume was run prior to the charging simulation, this is not to say that it was held static. Within the charging simulation domain, the field was still modified as the surface potential changed. This allowed for modifications in the plume shape. It was assumed that the plume far away from the panel (outside the charging domain) would be primarily main beam ions and would not be significantly affected by the surface charge. Potential changes would not be large enough to alter the velocity of far away CEX ions enough to accelerate them into the charging domain.

Since the plume simulation was large (to the extent that it was run in parallel), computational restraints prevented the entire domain being used for the charging simulation. For that reason, a portion of the solar array was chosen as the area to perform the charging calculation. This portion is shown

highlighted in Figure 4.6. The gradient applied to the panel ranges from $0 - 60V$. The domain used in the charging simulation was a box measuring $72cm$ away from all edges of the panel. Each grid square was $5cm$. The spacecraft was assumed to be conductive, except for the upper surface of the panel, which was given a conductivity of $1 \times 10^{-5} Sm^{-1}$ in the first case (Figure 4.8(b)) and a conductivity of $1 \times 10^{-10} Sm^{-1}$ (low enough to be considered nonconductive) in the second case (Figure 4.8(c))

The purpose of this test case is to show the effects on surface charging that are brought about by backflow from a thruster plume. Thruster plumes are more difficult to model than uniform ambient environments and few charging codes have accurate plume modeling.

v_b (km/s)	38.7
n_{b0} (cm^{-3})	3.22×10^9
v_{n0} (cm^{-3})	0.23×10^{12}
$\phi_{p0} - \phi_{sc}$ (V)	19
T_e (eV)	2.09

Table 4.5: Parameters for thruster plume deposition on panel test case

The results of the charging simulation are shown in Figure 4.8. As with the solar wind simulations from Section 4.2, the local spacecraft ground potential lowered significantly to balance out the potential gradient on the panel. Again like the solar wind test, the charge present at any given time in the surface helped to dull the effect of the gradient. The overall range was lowered by $18V$ for the case with the small conductivity, and the gradient was completely removed for the case with no conductivity.

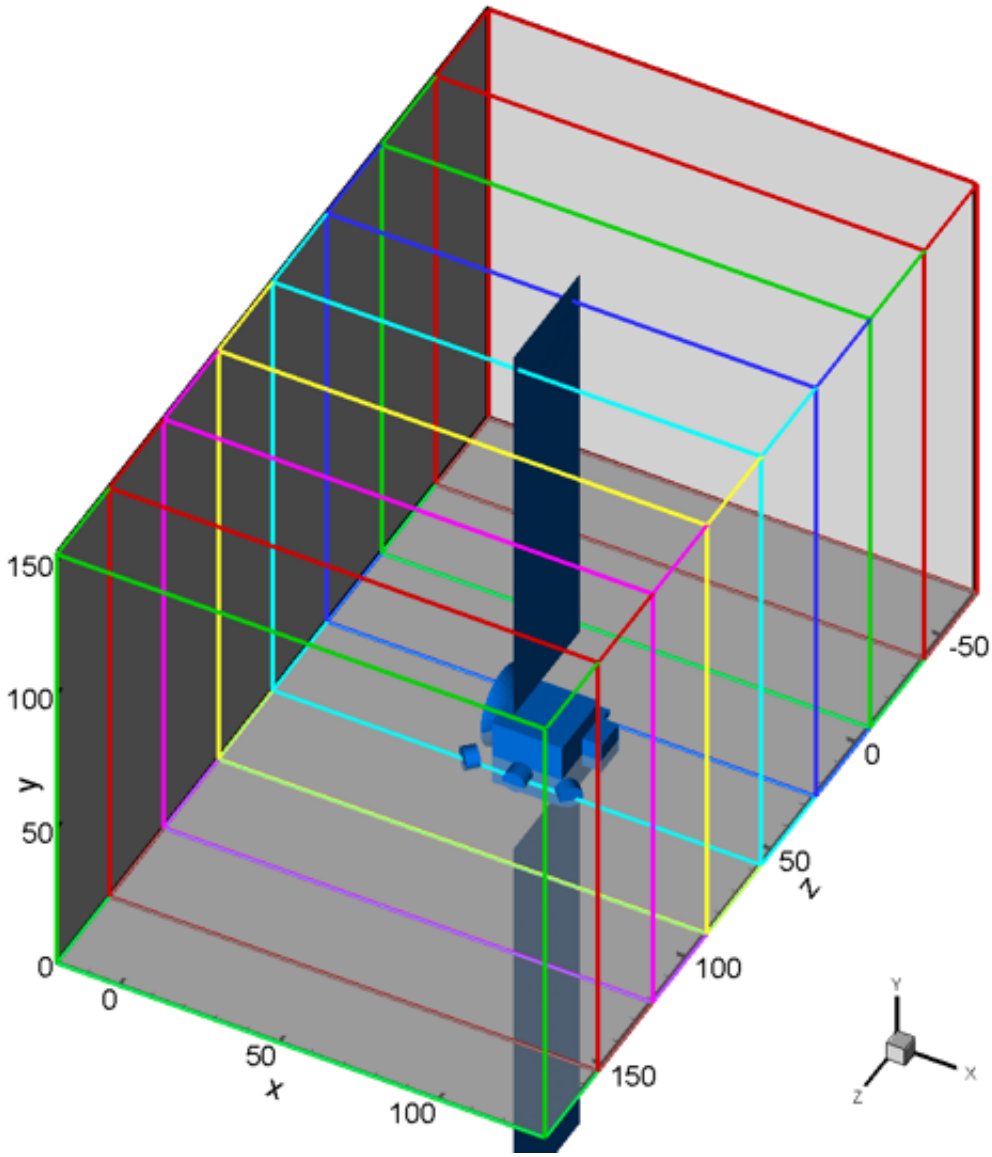

Figure 4.5: Geometry of thruster plume case, showing subdomains for parallel simulations[4]

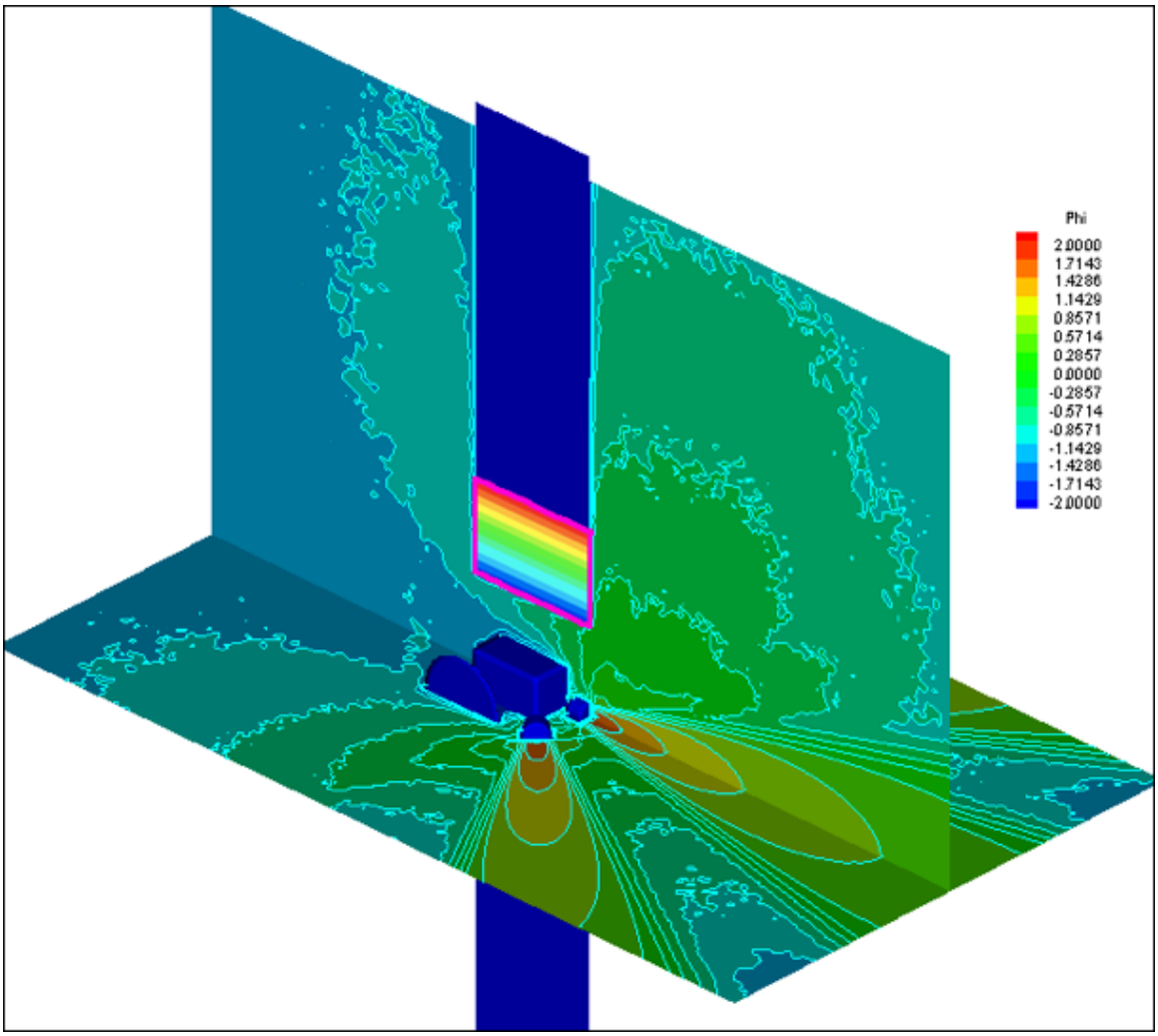

Figure 4.6: Potential of plume case, highlighting section of panel used in charging simulation. Gradient on panel ranges from $0-60V$. Plume potential taken from [4]

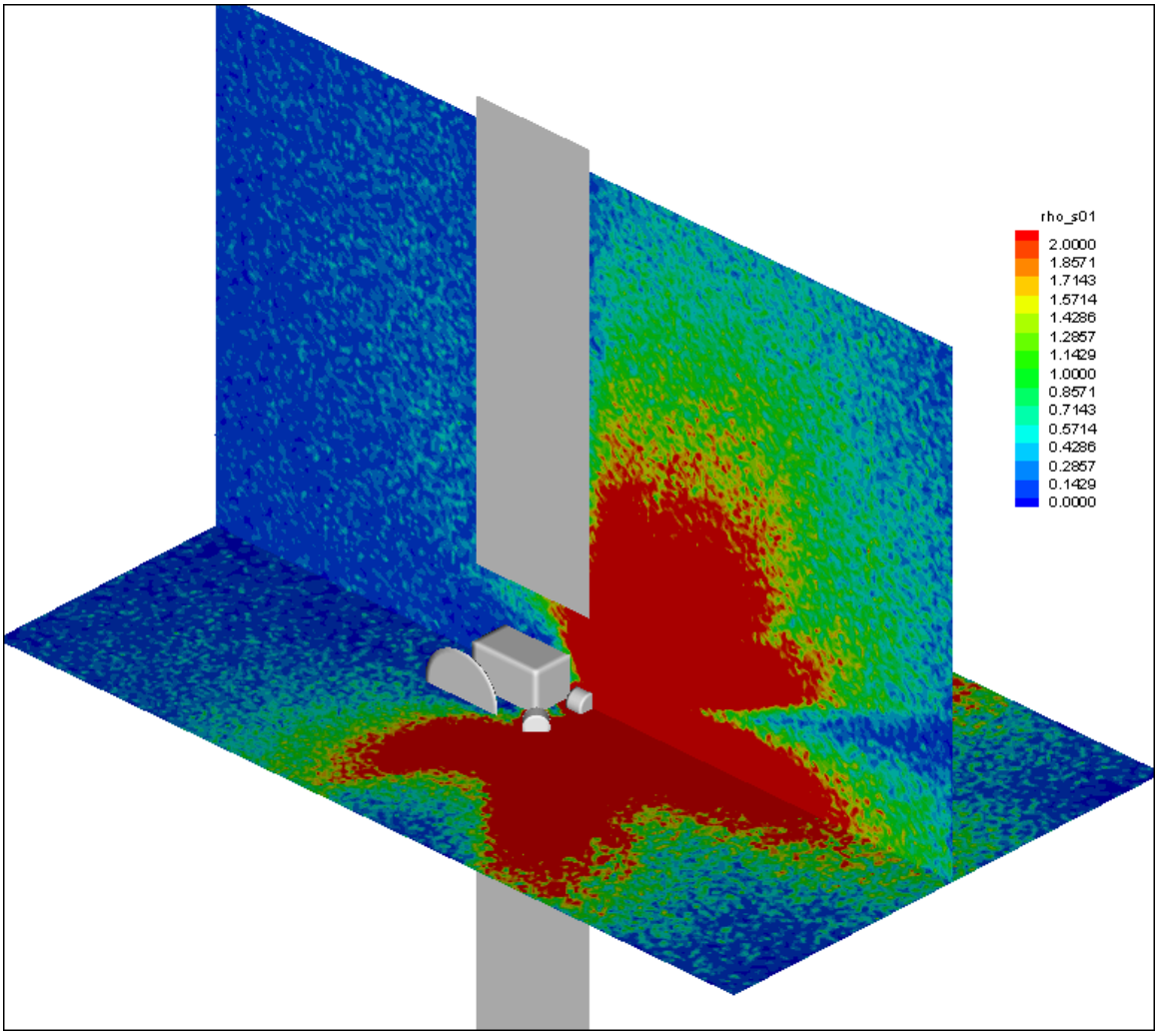

Figure 4.7: Number density of the plume used in the charging calculations[4]

The difference in this case is that a potential gradient also develops in the transverse direction. For the dielectric case, the driving gradient is removed, so the entire gradient is in the transverse direction. In the small conductivity case, however, the two gradients combine so that the overall potential gradient is on a 45 degree incline. This effect can be explained by looking at the plume plots in Figures 4.7 and 4.6.

The area of the panel closer to the thrusters (right side of the figure) has a lower potential than the areas far from the thrusters. This can be explained by looking at the shape of the thruster plume. The number density plot shown in Figure 4.7 shows a larger plume density closer to the thrusters and the potential plot shown in Figure 4.6 shows a more negative potential near the thrusters. This will lend to having more electrons in this area compared with other areas. If more electrons are to hit the surface, then the potential will be lower.

As shown, plume backflow from charge exchange ions can have a profound effect on the surface potential of a spacecraft. Potential gradients can appear both in the applied gradient direction, and perpendicular to it. This result makes it all the more necessary to model charging interactions when designing a spacecraft.

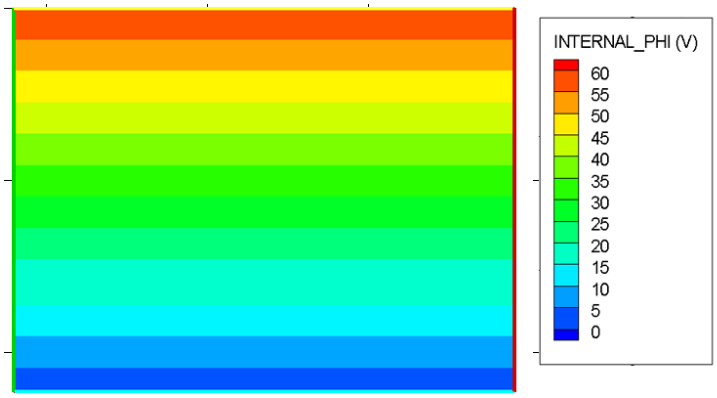

(a) Initial setup.

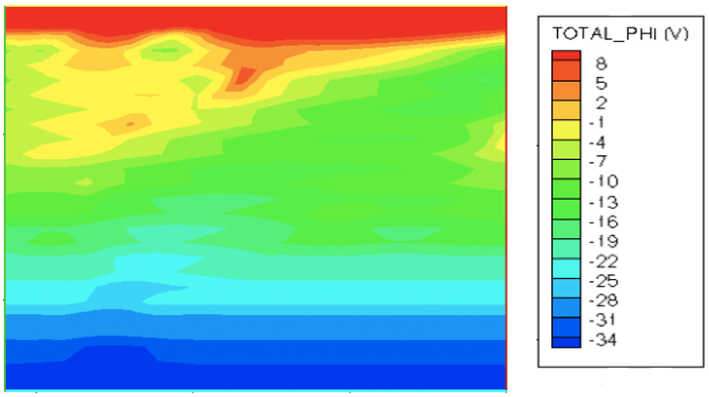

(b) Charging results for panel section in thruster plume environment with small conductivity.

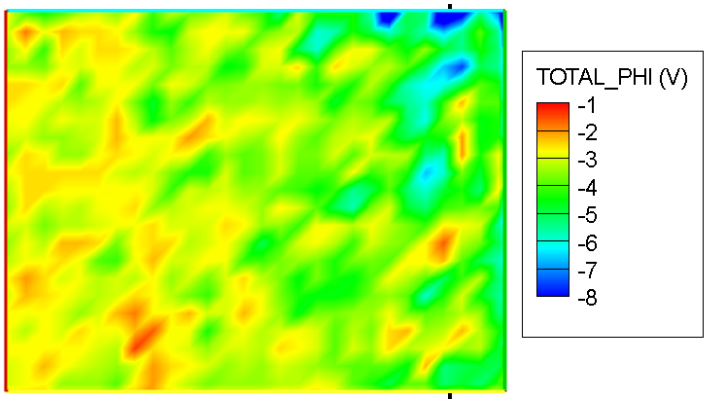

(c) Charging results for panel section in thruster plume environment with no conductivity.

Figure 4.8: Results for charging of panel element in plume environment.

Chapter 5

Summary and Conclusion

5.1 Conclusion

A spacecraft's potential is determined by charge accumulation. Since there is no practical way to test a spacecraft in space to see what potential gradients may appear, simulations are required to aid designers when planning for charging effects. Many codes have been developed to model these effects, however most use simplistic spacecraft and plume models. This work shows a new code that includes geometrically and conductively complex composite spacecraft for use in charging calculations. It is paired with t highly accurate plasma code used for solving thruster plumes.

The code developed is a new module for the DRACO code, which is an element of the overall COLISEUM framework, being developed for the Air Force. The code can be run either as a full PIC, modeling both ions and

electrons, or as a hybrid PIC, modeling ions and using a fluid Boltzmann electron model. The Boltzmann model was shown to be accurate for negative potentials, but inaccurate for large positive potentials. For this reason, the full PIC mode was used for the simulations in this work.

The algorithm takes charge and then redistributes it along the surface. This is done by solving the electric field inside the surface. Charge can move into the interior of the spacecraft where it can be added to the overall ground potential of the spacecraft. It can also be moved into neighboring surface cells. A system of time management is also in place to ensure accurate results while keeping computation time to a minimum.

Three test cases were run. The first case shows plume impingement of a spherical probe by a xenon thruster. This case illustrates the various modes in which the code can be run. It first illustrates a nonconductive mode, that simulates dielectric surfaces. These types of surfaces were shown to generate large gradients since charge cannot be transferred into equilibrium. A second mode with charge conducting over and through the surface was shown via a small amount of conductivity introduced into the probe's surface material, where charge reaching the interior was removed. This lowered the magnitude of the surface potential by a large amount, but the overall shape remained largely the same. The third mode showed the same sphere as in mode two, but now with a conductive interior. The conductive interior redistributed the charge to all parts of the probe evenly. This showed that a small conductivity may be sufficient to achieve a uniform potential map if the interior of the

spacecraft can be conductive.

The second test case shows a compositespacecraft exposed to the solar wind. This case was included to show the different effects that materials can have on the simulation as well as to show the effect of induced potential gradients. the spacecraft was tested with combinations of conductive, semiconductive, and nonconductive materials. A gradient was applied on a portion of the spacecraft as well. It was shown that the spacecraft will always reach an equilibrium state where electron current and ion current are balanced. If the spacecraft is largely conductive, this gradient will be shown in the overall surface potential map and the ground potential will lower to account for it. As the material becomes less conductive, the effect of the gradient also lessens as the elements on the surface begin to individually hold charge and balance against the ambient environment. Finally, with a nonconductive material, the gradient disappears completely and the entirespacecraft balances each element individually against the ambient environment.

The third test case shows a spacecraft firing a thruster. Charge exchange ions backflow towards the spacecraft. This case illustrates that nonuniform plasma environments, such as a CEX plume, can lead to potential gradients on the spacecraft surface. A transverse gradient, perpendicular to the applied gradient, appeared in this case because of the difference in plasma density and potential in the areas near the spacecraft.

This code module will soon be fully integrated into the DRACO code and COLISEUM framework and used on a regular basis to perform charging

calculations and to attain more accurate results for all plasma simulations.

5.2 Future Work

Several aspects of charging and general surface interactions were not completed by the writing of this thesis. They will be integrated in future work and are discussed here.

- There is currently no quick way to get a numerical value for the floating potential of a spacecraft. It can be inferred from the potential map, but is not calculated directly. A method to calculate the exact floating potential, possibly using the capacitance method, will need to be integrated in the future.

- Currently, the spacecraft body capacitance must be known in order to accurately calculate the spacecraft ground potential. A routine for approximating this value can be incorporated in the future.

- DRACO has the capacity to run as a parallel code. This has not yet, however, been integrated into the charging routine. Parallel processing would make simulations such as the plume[43] used in Section 4.3 able to run locally with the charging code instead of having to run the plume simulation first.

- The Boltzmann electron model used here is only accurate under certain conditions. Research into a more accurate fluid electron model needs to be carried out.

- The surface interaction package is currently limited. Support for sputtering, arcing, surface degradation, and a variety of new surface collision models will need to be added in the future.

Bibliography

[1] Material used with permission from AFRL.

[2] L. Breida, R. Kafafy, J. Pierru, and J. Wang. Development of the draco code for modeling electric propulsion plume interactions. In *40th AIAA/ASME/SAE/ASEE Joint Propulsion Conference & Exhibit*, July 2004.

[3] R. Kafafy and J. Wang. A hybrid grid immersed finite element particle in cell algorithm for modeling spacecraft plasma interactions. *IEEE Trans. Plasma Science*, 2006. accepted.

[4] J. Wang, Y. Cao, R. Kafafy, J. Pierru, and V. Decyk. Simulations of ion thruster plume spacecraft interactions on parallel supercomputer. *IEEE Trans. Plasma Science*, 2006. accepted.

[5] H. Garret. The charging of spacecraft surfaces. *Rev. Geophysics*, 19, 1981.

[6] E. Whipple. The equilibrium electric potential of a body in the upper atmosphere. In *NASA X-615-65-296*, 1965.

[7] S. DeForest. Spacecraft charging at synchronous orbit. *Journal of Geophysical Research*, 77, 1972.

[8] J. Jemiola. Spacecraft contamination: A review. *Space Systems and Their Interactions With the Earth's Space Environment*, 71, 1980.

[9] R. Grard. Properties of the satellite photoelectron sheath derived from photoemission laboratory experiments. *Journal of Geophysical Research*, 78, 1973.

[10] A. Lucas. Fundamental processes in particle and photon interactions with surfaces. In *Photon and Particle Interactions With Surfaces in Space*, 1973.

[11] I. Katz et al. The importance of accurate secondary electron yields in modeling spacecraft charging. *Journal of Geophysical Research*, 91, 1986.

[12] K. Balmain. Surface charging effects. *Space Systems and Their Interactions With the Earth's Space Environment*, 71, 1980.

[13] D. Hastings, M. Cho, and P. Chang. Interactions between a plasma flow and a highly biased solar array. In *25th Joint Propulsion Conference*, July 1989.

[14] J. Nanevicz and R. Adamo. Occurrence of arcing and its effect on space systems. *Space Systems and Their Interactions With the Earth's Space Environment*, 71, 1980.

[15] M. Leung and H. Kan. Laboratory study of the charging of spacecraft materials. *Journal of Spacecraft and Rockets*, 18, 1981.

[16] T. Kazuhiro et al. Degradation of high-voltage solar array due to arcing in plasma environment. *Journal of Spacecraft and Rockets*, 42, 2005.

[17] D. E. Hastings, M. Cho, and Ilitoshi Kuninakaf. The arcing rate for a high voltage solar array: Theory, experiment and predictions. In *30th Aerospace Sciences Meeting and Exhibit*, January 1992.

[18] M. Cho and G. Hastings. Computer particle simulation solar array arcing of high-voltage onset. *Journal of Spacecraft and Rockets*, 30, 1993.

[19] C. Brundin. Effects of charged particles on the motion of an earth satellite. *AIAA Journal*, 1, 1963.

[20] R. Bourdeau. On the interaction between a spacecraft and an ionized medium. *Space Science Review*, 1, 1963.

[21] A. Whittlesey and P. Leung. Space plasma charging - lessons from voyager. In *AlAA 25th Aerospace Sciences Meeting*, January 1987.

[22] C. Purvis et al. Design guidelines for assessing and controlling spacecraft charging effects. In *NASA Technical Paper 2361*, 1984.

[23] A. Frederickson et al. Characteristics of spontanious electrical discharges of various insulators in space radiation. *IEEE Transactions on Nuclear Science*, 39(6), 1982.

[24] H. Garret and A. Whittlesey. Spacecraft charging, an update. In *AIAA-96-0143*, 1996.

[25] H. Garret. Future directions in spacecraft charging-2001 and beyond. In *AIAA-2002-0624*, 2002.

[26] C. Birdsall and A. Langdon. *Plasma Physics via Computer Simulation*. Taylor & Francis, 2004.

[27] I. Katz et al. A three dimensional study of electrostatic charging in materials. In *NASA Rep.*, CR-135256, August 1977.

[28] I. Katz and Mandell M. J. High voltage plasma interactions using nascap/leo. In *20th Aerospace Sciences Meeting*, AIAA-90-0725, January 1990.

[29] M. J. Mandell et al. Nascap2k - spacecraft charging analysis code for the 21st century. In *39th Aerospace Sciences Meeting and Exhibit*, AIAA 01–957, Reno, Nevada, January 2001.

[30] M. J. Mandell et al. Modeling the charging of geosynchronous and interplanetary spacecraft using nascap-2k. *Advances in Space Research*, 36, 2005.

[31] M.J. Mandell, T. Luu, J. Lilley, G. Jongeward, and I. Katz. Analysis of dynamical plasma interactions with high voltage spacecraft. In *Phillips Lab*, Rep. PL-TR-92-2258, June 1992.

[32] I. Mikellides, M. Mandell, R. Kuharski, and B. Gardner. The electric propulsion interactions code (epic): A member of the nasa see program toolset. In *39th AIAA/ASME/SAE/ASEE Joint Propulsion Conference and Exhibit*, July 2003.

[33] K. Kannenberg and I. Boyd. Development of a 3d parallel dsmc code for plume impingement studies. In *AIAA Thermophysics Conference*, June 1996.

[34] D. Oh and D. Hastings. Three dimensional pic-dsmc simulations of hall thruster plumes and analysis for realistic spacecraft configurations. In *32nd AIAA/ASME/SAE/ASEE Joint Propulsion Conference and Exhibit*, July 1996.

[35] D. Oh and D. Hastings. Experimental verification of a pic-dsmc model for hall thruster plumes. In *32nd AIAA/ASME/SAE/ASEE Joint Propulsion Conference and Exhibit*, July 1996.

[36] D. VanGilder, M. Keidar, and I. Boyd. Modeling hall thruster plumes using particle methods. In *35th AIAA/ASME/SAE/ASEE Joint Propulsion Conference and Exhibit*, July 1999.

[37] J. Fife et al. The development of a flexible, usable plasma interaction modeling system. In *38th AIAA/ASME/SAE/ASEE Joint Propulsion Conference & Exhibit*, July 2002.

[38] J. Koo and I. Boyd. Computational modeling of stationary plasma thrusters. In *39th AIAA/ASME/SAE/ASEE Joint Propulsion Conference & Exhibit*, July 2003.

[39] J. Wang, D. Brinza, and M. Young. Three-dimensional particle simulations of ion propulsion plasma environment for deep space 1. *Journal of Spacecraft and Rockets*, 38(3), 2001.

[40] C. Scharlemann, M. Tajmar, and and D. Estublier J. Gonzalez. Influence of the solar arrays on the floating potential of smart-1: Numerical simulations. In *41st AIAA/ASME/SAE/ASEE Joint Propulsion Conference & Exhibit*, July 2005.

[41] M. Tajmar, J. Gonzalez, and A. Hilgers. Modeling of spacecraftenvironment interactions on smart-1. *Journal of Spacecraft and Rockets*, 38(3), 2001.

[42] J. Gonzalez del Amo et al. Smart-1: Spacecraft/thruster interaction data analysis. *4th International Spacecraft Propulsion Conference*, June 2004.

[43] J. Wang, Y. Cao, and R. Kafafy. Ion impingement limits of subscale ion optics: Comparisons of simulation and experiment. In *42nd AIAA/ASME/SAE/ASEE Joint Propulsion Conference and Exhibit*, July 2006.

[44] J. Roussel, F. Rogier, D. Volpert, G. Rousseau, J. Forest, and A. Hilgers. Spacecraft plasma interaction software (spis): numerical solvers methods and architecture. In *9th Spacecraft Charging Technology Conference*, April 2005.

[45] A. Hilgers, J. Thiebault, J. Roussel, J Forest, and E. Engwall. Tests and validation of a new spacecraft plasma interaction software, spis. In *9th Spacecraft Charging Technology Conference*, April 2005.

[46] D. Hewett, W. Larson, and S. Doss. Solution of simultaneous partial differerential equations using dynamic adi: Solution of the streamline darwin field equations. *Journal of Computational Physics*, 101, 1992.

[47] R. Kafafy, T. Lin, Y. Lin, and J. Wang. 3-d immersed finite element method for electric field simulation in composite materials. *Int. Journal for Numerical Methods in Engineering*, 64, 2005.

[48] L. Brieda. Development of the draco es-pic code and fully-kinetic simulation of ion beam neutralization. In *Masters Thesis*, 2005. Virginia Tech.

[49] S. M. L. Prokopenko and J. G. Laframboise. High voltage differential charging of geostationary spacecraft. *Journal of Geophysical Research*, 85(4125), 1980.

[50] L. Brieda and D. VanGilder. Multi-domain plasma expansion simulations using a particle-in-cell method. In *42nd AIAA/ASME/SAE/ASEE Joint Propulsion Conference & Exhibit*, July 2006.

[51] M. Rayman. Preparing for the dawn mission to vesta and ceres. In *56th International Astronautical Congress of the International Astronautical Federation, the International Academy of Astronautics, and the International Institute of Space Law*, October 2005.

Appendix A
Sample coliseum.in File

```
# set the zone curvature parameter
set surface_zone_angle_min 0.7679

# set detailed viewability
#set full_view 1

#load material information
component_load component.txt
material_load material.txt mat_mat.txt

#load satellite
surface_load ANSYS sphere.ans
surface_load ANSYS panel.ans
surface_load ANSYS source.ans

surface_save TECPLOT surface.dat

#simulation parameters
SET dt 5e-11
SET nt 30000
SET nt_restart_save 100
SET nt_field_update 1
set dhp_per_step 0.6

#set simulation space
#volcar domain.txt
```

```
#volcar_save mesh.v
volcar_load mesh.v

#setup sources
source_specify SW MAXSTREAM e 38e-19 4.6440e+05 400e3 0
source_specify SW MAXSTREAM O+ 7.7556e-15 1.1610e+05 400e3 0
source_specify SW FILE O+ O+ 0 0 1 o.dat
source_specify SW FILE O+ e 0 0 1 o.dat

#set reference temperature in eV (i.e. kT/e), T=14506K
SET Te_Ref 40

#set reference potential in V
SET Phi_Ref 0

#set reference electron density
SET Ne_Ref 350000

#set normalization specie
SET Specie_Ref e

#set solver
draco_init_solver dadi linear 500 1e-3

#set charging parameters
SET nt_charging 1

draco_init_charging 1 100000000000 -100 0 0 0 27.78e-6

#run draco
draco

#save output info
volcar_mesh_save TECPLOT field2.dat phi rho nd.e nd.O+

draco_particle_save particles.dat ALL O+ 1
draco_particle_save append ALL e 1
```

Appendix B
Sample material.txt File

name	flying	molwt	spwt	charge	density	permittivity	conductivity
Xe+	yes	131.4	4e8	1	1e4	0	0
Al	no	26.9	0	0	2700	0.00001	1e10
O	yes	16	1	0	1e12	0.00001	1e-6
O+	yes	16	100	1	1e12	0.00001	1e-6
e	yes	5.5e-4	100	-1	1e12	0	0
glass	no	10	1	0	2700	6e-11	1e-10
silicon	no	28.08	1	0	2700	6e-9	1e-3

Appendix C
Sample mat_mat.txt File

```
target source sticking_c sputter_model sputter_c1 sputter_c2 sputter_c3
sputter_c4 sputter_c5
bus Xe+ 0 roussel 1 1.9E+16 0 0 0
```

Appendix D
Sample component.txt File

Name	Num	mat_name	phi	eps	type	thickness
backing	1	Al	0	100000	solid	0
SW	2	Al	0	1	source	0
glass	3	Al	0	100000	solid	0
craft	4	Al	0	100000	solid	0

Appendix E
Sample domain.txt File

```
add_grid
 x0: 0
 y0: 0
 z0: 0
 dx: .05
 dy: .05
 dz: .05
 nx: 92
 ny: 70
 nz: 70

 set_boundary X_MIN NEUMANN 0
 set_boundary X_MAX NEUMANN 0
 set_boundary Y_MIN NEUMANN 0
 set_boundary Y_MAX NEUMANN 0
 set_boundary Z_MIN DIRICHLET 0
 set_boundary Z_MAX NEUMANN 0
end_grid
```

Appendix F
Sample Charging Input File

```
VARIABLES = "x (m)", "y (m)", "z (m)", "node_num", "normal_x", "normal_y", "normal_z", area, "SURFACE_PHI (V)", "TOTAL_PHI (V)", "INTERNAL_PHI (V)"

ZONE F=FEPOINT, N=122, NV=4, E=240, ET=TRIANGLE, T=CRAFT
     1.75     1.75       2 1       0  3.16827e-10       1  0.00501311       0       0       0
    1.8204     1.75    1.9899 2   0.300033   0.0150279    0.95381  0.00248344       0       0       0
    1.811    1.7852    1.9899 3    0.25237   0.162947   0.953812  0.00248465       0       0       0
    1.7852     1.811    1.9899 4   0.136891   0.267389   0.953816  0.00248456       0       0       0
     1.75    1.8204    1.9899 5  -0.0150279   0.300033    0.95381  0.00248344       0       0       0
    1.7148     1.811    1.9899 6   -0.162947    0.25237   0.953812  0.00248465       0       0       0
    1.689    1.7852    1.9899 7   -0.267389   0.136891   0.953816  0.00248456       0       0       0
    1.6796     1.75    1.9899 8   -0.300033  -0.0150279    0.95381  0.00248344       0       0       0
    1.689    1.7148    1.9899 9   -0.25237   -0.162947   0.953812  0.00248465       0       0       0
    1.7148     1.689    1.9899 10   -0.136891   -0.267389   0.953816  0.00248456       0       0       0
     1.75    1.6796    1.9899 11   0.0150279   -0.300033    0.95381  0.00248344       0       0       0
    1.7852     1.689    1.9899 12   0.162947   -0.25237   0.953812  0.00248465       0       0       0
    1.811    1.7148    1.9899 13   0.267389   -0.136891   0.953816  0.00248456       0       0       0
    1.8852     1.75    1.9603 14   0.548898   0.0148534   0.835758  0.00479901       0       0       0
    1.8671    1.8176    1.9603 15   0.467892   0.287202   0.835818  0.00479872       0       0       0
    1.8176    1.8671    1.9603 16   0.261501   0.482792   0.835781  0.00480007       0       0       0
     1.75    1.8852    1.9603 17  -0.0148534   0.548897   0.835758  0.00479901       0       0       0
    1.6824    1.8671    1.9603 18   -0.287202   0.467892   0.835818  0.00479872       0       0       0
    1.6329    1.8176    1.9603 19   -0.482792   0.261501   0.835781  0.00480007       0       0       0
    1.6148     1.75    1.9603 20   -0.548897  -0.0148534   0.835758  0.00479901       0       0       0
    1.6329    1.6824    1.9603 21   -0.467892   -0.287202   0.835818  0.00479872       0       0       0
    1.6824    1.6329    1.9603 22   -0.261501   -0.482792   0.835781  0.00480007       0       0       0
     1.75    1.6148    1.9603 23   0.0148534   -0.548897   0.835758  0.00479901       0       0       0
    1.8176    1.6329    1.9603 24   0.287202   -0.467892   0.835818  0.00479872       0       0       0
    1.8671    1.6824    1.9603 25   0.482792   -0.261501   0.835781  0.00480007       0       0       0
    1.9389     1.75    1.9137 26   0.759122   0.0114629   0.650847  0.00676471       0       0       0
    1.9136    1.8445    1.9137 27   0.651884   0.389477   0.650657  0.00676069       0       0       0
    1.8445    1.9136    1.9137 28   0.369748   0.663164   0.650769  0.00676251       0       0       0
     1.75    1.9389    1.9137 29  -0.0114629   0.759122   0.650847  0.00676471       0       0       0
    1.6555    1.9136    1.9137 30   -0.389477   0.651884   0.650657  0.00676069       0       0       0
    1.5864    1.8445    1.9137 31   -0.663164   0.369748   0.650769  0.00676251       0       0       0
    1.5611     1.75    1.9137 32   -0.759122  -0.0114629   0.650847  0.00676471       0       0       0
    1.5864    1.6555    1.9137 33   -0.651884   -0.389477   0.650657  0.00676069       0       0       0
    1.6555    1.5864    1.9137 34   -0.369748   -0.663164   0.650769  0.00676251       0       0       0
     1.75    1.5611    1.9137 35   0.0114629   -0.759122   0.650847  0.00676471       0       0       0
    1.8445    1.5864    1.9137 36   0.389477   -0.651884   0.650657  0.00676069       0       0       0
    1.9136    1.6555    1.9137 37   0.663164   -0.369748   0.650769  0.00676251       0       0       0
    1.9774     1.75    1.8539 38   0.910515  0.00728948   0.413411  0.00821279       0       0       0
    1.9469    1.8637    1.8539 39   0.785054   0.461614    0.41304  0.00821095       0       0       0
    1.8637    1.9469    1.8539 40   0.449283   0.792187    0.41302  0.00820877       0       0       0
     1.75    1.9774    1.8539 41  -0.00728947   0.910515   0.413411  0.00821278       0       0       0
    1.6363    1.9469    1.8539 42   -0.461614   0.785054    0.41304  0.00821095       0       0       0
    1.5531    1.8637    1.8539 43   -0.792187   0.449283    0.41302  0.00820877       0       0       0
    1.5226     1.75    1.8539 44   -0.910515  -0.00728947   0.413411  0.00821278       0       0       0
    1.5531    1.6363    1.8539 45   -0.785054   -0.461614    0.41304  0.00821095       0       0       0
    1.6363    1.5531    1.8539 46   -0.449283   -0.792187    0.41302  0.00820877       0       0       0
     1.75    1.5226    1.8539 47  0.00728947   -0.910515   0.413411  0.00821278       0       0       0
    1.8637    1.5531    1.8539 48   0.461614   -0.785054    0.41304  0.00821095       0       0       0
    1.9469    1.6363    1.8539 49   0.792187   -0.449283    0.41302  0.00820877       0       0       0
    1.9975     1.75    1.7856 50   0.989906  0.00248532   0.141707   0.008984       0       0       0
    1.9643    1.8737    1.7856 51   0.855996   0.497221   0.141573  0.00898555       0       0       0
```

```
    1.8737    1.9643    1.7856 52    0.493011    0.858438    0.141508  0.00898408        0        0        0
     1.75    1.9975    1.7856 53  -0.00248532    0.989905    0.141707    0.008984        0        0        0
    1.6263    1.9643    1.7856 54    -0.497221    0.855996    0.141573  0.00898555        0        0        0
    1.5357    1.8737    1.7856 55    -0.858438    0.493011    0.141508  0.00898408        0        0        0
    1.5025     1.75    1.7856 56    -0.989905  -0.00248532    0.141707    0.008984        0        0        0
    1.5357    1.6263    1.7856 57    -0.855996    -0.497221    0.141573  0.00898555        0        0        0
    1.6263    1.5357    1.7856 58    -0.493011    -0.858438    0.141508  0.00898408        0        0        0
     1.75    1.5025    1.7856 59   0.00248532    -0.989905    0.141707    0.008984        0        0        0
    1.8737    1.5357    1.7856 60    0.497221    -0.855996    0.141573  0.00898555        0        0        0
    1.9643    1.6263    1.7856 61    0.858438    -0.493011    0.141508  0.00898408        0        0        0
    1.9975     1.75    1.7144 62    0.989906  -0.00248532    -0.141707    0.008984        0        0        0
    1.9643    1.8737    1.7144 63    0.858438    0.493011    -0.141508  0.00898407        0        0        0
    1.8737    1.9643    1.7144 64    0.497221    0.855996    -0.141573  0.00898555        0        0        0
     1.75    1.9975    1.7144 65   0.00248532    0.989905    -0.141707    0.008984        0        0        0
    1.6263    1.9643    1.7144 66    -0.493011    0.858438    -0.141508  0.00898407        0        0        0
    1.5357    1.8737    1.7144 67    -0.855996    0.497221    -0.141573  0.00898555        0        0        0
    1.5025     1.75    1.7144 68    -0.989905   0.00248532    -0.141707    0.008984        0        0        0
    1.5357    1.6263    1.7144 69    -0.858438    -0.493011    -0.141508  0.00898407        0        0        0
    1.6263    1.5357    1.7144 70    -0.497221    -0.855996    -0.141573  0.00898555        0        0        0
     1.75    1.5025    1.7144 71  -0.00248532    -0.989905    -0.141707    0.008984        0        0        0
    1.8737    1.5357    1.7144 72    0.493011    -0.858438    -0.141508  0.00898407        0        0        0
    1.9643    1.6263    1.7144 73    0.855996    -0.497221    -0.141573  0.00898555        0        0        0
    1.9774     1.75    1.6461 74    0.910515  -0.00728948    -0.413411  0.00821278        0        0        0
    1.9469    1.8637    1.6461 75    0.792187    0.449283    -0.41302  0.00820877        0        0        0
    1.8637    1.9469    1.6461 76    0.461614    0.785054    -0.41304  0.00821095        0        0        0
     1.75    1.9774    1.6461 77   0.00728948    0.910515    -0.413411  0.00821279        0        0        0
    1.6363    1.9469    1.6461 78    -0.449283    0.792187    -0.41302  0.00820877        0        0        0
    1.5531    1.8637    1.6461 79    -0.785054    0.461614    -0.41304  0.00821095        0        0        0
    1.5226     1.75    1.6461 80    -0.910515   0.00728948    -0.413411  0.00821279        0        0        0
    1.5531    1.6363    1.6461 81    -0.792187    -0.449283    -0.41302  0.00820877        0        0        0
    1.6363    1.5531    1.6461 82    -0.461614    -0.785054    -0.41304  0.00821095        0        0        0
     1.75    1.5226    1.6461 83   -0.00728948    -0.910515    -0.413411  0.00821279        0        0        0
    1.8637    1.5531    1.6461 84    0.449283    -0.792187    -0.41302  0.00820877        0        0        0
    1.9469    1.6363    1.6461 85    0.785054    -0.461614    -0.41304  0.00821095        0        0        0
    1.9389     1.75    1.5863 86    0.759122  -0.0114629    -0.650847  0.00676471        0        0        0
    1.9136    1.8445    1.5863 87    0.663164    0.369748    -0.650768  0.00676251        0        0        0
    1.8445    1.9136    1.5863 88    0.389477    0.651884    -0.650657  0.00676069        0        0        0
     1.75    1.9389    1.5863 89   0.0114629    0.759122    -0.650847  0.00676471        0        0        0
    1.6555    1.9136    1.5863 90    -0.369748    0.663164    -0.650768  0.00676251        0        0        0
    1.5864    1.8445    1.5863 91    -0.651884    0.389477    -0.650657  0.00676069        0        0        0
    1.5611     1.75    1.5863 92    -0.759122   0.0114629    -0.650847  0.00676471        0        0        0
    1.5864    1.6555    1.5863 93    -0.663164    -0.369748    -0.650768  0.00676251        0        0        0
    1.6555    1.5864    1.5863 94    -0.389477    -0.651884    -0.650657  0.00676069        0        0        0
     1.75    1.5611    1.5863 95   -0.0114629    -0.759122    -0.650847  0.00676471        0        0        0
    1.8445    1.5864    1.5863 96    0.369748    -0.663164    -0.650768  0.00676251        0        0        0
    1.9136    1.6555    1.5863 97    0.651884    -0.389477    -0.650657  0.00676069        0        0        0
    1.8852     1.75    1.5397 98    0.548898  -0.0148534    -0.835758  0.00479901        0        0        0
    1.8671    1.8176    1.5397 99    0.482792    0.261501    -0.835781  0.00480007        0        0        0
    1.8176    1.8671    1.5397 100    0.287202    0.467892    -0.835818  0.00479872        0        0        0
     1.75    1.8852    1.5397 101   0.0148534    0.548898    -0.835758  0.00479901        0        0        0
    1.6824    1.8671    1.5397 102    -0.261501    0.482792    -0.835781  0.00480007        0        0        0
    1.6329    1.8176    1.5397 103    -0.467892    0.287202    -0.835818  0.00479872        0        0        0
    1.6148     1.75    1.5397 104    -0.548898   0.0148534    -0.835758  0.00479901        0        0        0
    1.6329    1.6824    1.5397 105    -0.482792    -0.261501    -0.835781  0.00480007        0        0        0
    1.6824    1.6329    1.5397 106    -0.287202    -0.467892    -0.835818  0.00479872        0        0        0
     1.75    1.6148    1.5397 107  -0.0148534    -0.548898    -0.835758  0.00479901        0        0        0
    1.8176    1.6329    1.5397 108    0.261501    -0.482792    -0.835781  0.00480007        0        0        0
    1.8671    1.6824    1.5397 109    0.467892    -0.287202    -0.835818  0.00479872        0        0        0
    1.8204     1.75    1.5101 110    0.300033  -0.0150279    -0.95381  0.00248344        0        0        0
    1.811    1.7852    1.5101 111    0.267389    0.136891    -0.953816  0.00248456        0        0        0
    1.7852     1.811    1.5101 112    0.162947     0.25237    -0.953812  0.00248465        0        0        0
     1.75    1.8204    1.5101 113   0.0150279    0.300033    -0.95381  0.00248344        0        0        0
    1.7148     1.811    1.5101 114    -0.136891    0.267389    -0.953816  0.00248456        0        0        0
    1.689    1.7852    1.5101 115    -0.25237    0.162947    -0.953812  0.00248465        0        0        0
    1.6796     1.75    1.5101 116    -0.300033   0.0150279    -0.95381  0.00248344        0        0        0
    1.689    1.7148    1.5101 117    -0.267389    -0.136891    -0.953816  0.00248456        0        0        0
    1.7148     1.689    1.5101 118    -0.162947    -0.25237    -0.953812  0.00248465        0        0        0
     1.75    1.6796    1.5101 119  -0.0150279    -0.300033    -0.95381  0.00248344        0        0        0
    1.7852     1.689    1.5101 120    0.136891    -0.267389    -0.953816  0.00248456        0        0        0
    1.811    1.7148    1.5101 121     0.25237    -0.162947    -0.953812  0.00248465        0        0        0
     1.75     1.75      1.5 122        0  1.90096e-09      -1  0.00501311        0        0        0
1 2 3
1 3 4
1 4 5
1 5 6
1 6 7
1 7 8
```

1 8 9
1 9 10
1 10 11
1 11 12
1 12 13
1 13 2
14 15 2
3 2 15
15 16 3
4 3 16
16 17 4
5 4 17
17 18 5
6 5 18
18 19 6
7 6 19
19 20 7
8 7 20
20 21 8
9 8 21
21 22 9
10 9 22
22 23 10
11 10 23
23 24 11
12 11 24
24 25 12
13 12 25
25 14 13
2 13 14
26 27 14
15 14 27
27 28 15
16 15 28
28 29 16
17 16 29
29 30 17
18 17 30
30 31 18
19 18 31
31 32 19
20 19 32
32 33 20
21 20 33
33 34 21
22 21 34
34 35 22
23 22 35
35 36 23
24 23 36
36 37 24
25 24 37
37 26 25
14 25 26
38 39 26
27 26 39
39 40 27
28 27 40
40 41 28
29 28 41
41 42 29
30 29 42
42 43 30
31 30 43
43 44 31
32 31 44
44 45 32
33 32 45
45 46 33
34 33 46
46 47 34
35 34 47
47 48 35
36 35 48
48 49 36
37 36 49
49 38 37

```
26 37 38
50 51 38
39 38 51
51 52 39
40 39 52
52 53 40
41 40 53
53 54 41
42 41 54
54 55 42
43 42 55
55 56 43
44 43 56
56 57 44
45 44 57
57 58 45
46 45 58
58 59 46
47 46 59
59 60 47
48 47 60
60 61 48
49 48 61
61 50 49
38 49 50
62 63 50
51 50 63
63 64 51
52 51 64
64 65 52
53 52 65
65 66 53
54 53 66
66 67 54
55 54 67
67 68 55
56 55 68
68 69 56
57 56 69
69 70 57
58 57 70
70 71 58
59 58 71
71 72 59
60 59 72
72 73 60
61 60 73
73 62 61
50 61 62
74 75 62
63 62 75
75 76 63
64 63 76
76 77 64
65 64 77
77 78 65
66 65 78
78 79 66
67 66 79
79 80 67
68 67 80
80 81 68
69 68 81
81 82 69
70 69 82
82 83 70
71 70 83
83 84 71
72 71 84
84 85 72
73 72 85
85 74 73
62 73 74
86 87 74
75 74 87
87 88 75
76 75 88
```

88 89 76
77 76 89
89 90 77
78 77 90
90 91 78
79 78 91
91 92 79
80 79 92
92 93 80
81 80 93
93 94 81
82 81 94
94 95 82
83 82 95
95 96 83
84 83 96
96 97 84
85 84 97
97 86 85
74 85 86
98 99 86
87 86 99
99 100 87
88 87 100
100 101 88
89 88 101
101 102 89
90 89 102
102 103 90
91 90 103
103 104 91
92 91 104
104 105 92
93 92 105
105 106 93
94 93 106
106 107 94
95 94 107
107 108 95
96 95 108
108 109 96
97 96 109
109 98 97
86 97 98
110 111 98
99 98 111
111 112 99
100 99 112
112 113 100
101 100 113
113 114 101
102 101 114
114 115 102
103 102 115
115 116 103
104 103 116
116 117 104
105 104 117
117 118 105
106 105 118
118 119 106
107 106 119
119 120 107
108 107 120
120 121 108
109 108 121
121 110 109
98 109 110
111 110 122
112 111 122
113 112 122
114 113 122
115 114 122
116 115 122
117 116 122
118 117 122
119 118 122

```
120 119 122
121 120 122
110 121 122

ZONE F=FEPOINT, N=231, NV=4, E=400, ET=TRIANGLE, T=GLASS
     2.1      1.5     1.75 123       0       0       1  0.000416668       0       0      2.8571428571428568
     2.1     1.55     1.75 124       0       0       1     0.00125       0       0      2.5974025974025974
     2.1      1.6     1.75 125       0       0       1  0.00125001       0       0      2.3376623376623376
     2.1     1.65     1.75 126       0       0       1     0.00125       0       0      2.0779220779220777
     2.1      1.7     1.75 127       0       0       1  0.00125001       0       0       1.818181818181818
     2.1     1.75     1.75 128       0       0       1     0.00125       0       0      1.5584415584415583
     2.1      1.8     1.75 129       0       0       1     0.00125       0       0      1.2987012987012987
     2.1     1.85     1.75 130       0       0       1  0.00125001       0       0      1.0389610389610389
     2.1      1.9     1.75 131       0       0       1     0.00125       0       0      0.7792207792207791
     2.1     1.95     1.75 132       0       0       1  0.00125001       0       0      0.5194805194805194
     2.1        2    1.75 133       0       0       1  0.000833336       0       0      0.2597402597402597
    2.15      1.5     1.75 134       0       0       1     0.00125       0       0      2.8571428571428568
    2.15     1.55     1.75 135       0       0       1      0.0025       0       0      3.1168831168831166
    2.15      1.6     1.75 136       0       0       1      0.0025       0       0      3.3766233766233764
    2.15     1.65     1.75 137       0       0       1      0.0025       0       0      3.636363636363636
    2.15      1.7     1.75 138       0       0       1      0.0025       0       0      3.8961038961038956
    2.15     1.75     1.75 139       0       0       1      0.0025       0       0      4.1558441558441555
    2.15      1.8     1.75 140       0       0       1      0.0025       0       0      4.415584415584415
    2.15     1.85     1.75 141       0       0       1      0.0025       0       0      4.675324675324675
    2.15      1.9     1.75 142       0       0       1      0.0025       0       0      4.9350649350649345
    2.15     1.95     1.75 143       0       0       1      0.0025       0       0      5.194805194805195
    2.15        2     1.75 144       0       0       1     0.00125       0       0      5.454545454545454
     2.2      1.5     1.75 145       0       0       1     0.00125       0       0      8.571428571428571
     2.2     1.55     1.75 146       0       0       1      0.0025       0       0      8.311688311688311
     2.2      1.6     1.75 147       0       0       1      0.0025       0       0      8.05194805194805
     2.2     1.65     1.75 148       0       0       1      0.0025       0       0      7.792207792207791
     2.2      1.7     1.75 149       0       0       1      0.0025       0       0      7.532467532467532
     2.2     1.75     1.75 150       0       0       1      0.0025       0       0      7.272727272727272
     2.2      1.8     1.75 151       0       0       1      0.0025       0       0      7.012987012987012
     2.2     1.85     1.75 152       0       0       1      0.0025       0       0      6.753246753246753
     2.2      1.9     1.75 153       0       0       1      0.0025       0       0      6.493506493506493
     2.2     1.95     1.75 154       0       0       1      0.0025       0       0      6.233766233766233
     2.2        2    1.75 155       0       0       1     0.00125       0       0      5.974025974025974
    2.25      1.5     1.75 156       0       0       1     0.00125       0       0      8.571428571428571
    2.25     1.55     1.75 157       0       0       1      0.0025       0       0      8.83116883116883
    2.25      1.6     1.75 158       0       0       1      0.0025       0       0      9.09090909090909
    2.25     1.65     1.75 159       0       0       1      0.0025       0       0      9.35064935064935
    2.25      1.7     1.75 160       0       0       1      0.0025       0       0      9.610389610389609
    2.25     1.75     1.75 161       0       0       1      0.0025       0       0      9.870129870129869
    2.25      1.8     1.75 162       0       0       1      0.0025       0       0      10.12987012987013
    2.25     1.85     1.75 163       0       0       1      0.0025       0       0      10.38961038961039
    2.25      1.9     1.75 164       0       0       1      0.0025       0       0      10.649350649350648
    2.25     1.95     1.75 165       0       0       1      0.0025       0       0      10.909090909090908
    2.25        2     1.75 166       0       0       1     0.00125       0       0      11.168831168831169
     2.3      1.5     1.75 167       0       0       1     0.00125       0       0      14.285714285714285
     2.3     1.55     1.75 168       0       0       1      0.0025       0       0      14.025974025974024
     2.3      1.6     1.75 169       0       0       1      0.0025       0       0      13.766233766233764
     2.3     1.65     1.75 170       0       0       1      0.0025       0       0      13.506493506493506
     2.3      1.7     1.75 171       0       0       1      0.0025       0       0      13.246753246753245
     2.3     1.75     1.75 172       0       0       1      0.0025       0       0      12.987012987012985
     2.3      1.8     1.75 173       0       0       1      0.0025       0       0      12.727272727272727
     2.3     1.85     1.75 174       0       0       1      0.0025       0       0      12.467532467532466
     2.3      1.9     1.75 175       0       0       1      0.0025       0       0      12.207792207792206
     2.3     1.95     1.75 176       0       0       1      0.0025       0       0      11.948051948051948
     2.3        2    1.75 177       0       0       1     0.00125       0       0      11.688311688311687
    2.35      1.5     1.75 178       0       0       1     0.00125       0       0      14.285714285714285
    2.35     1.55     1.75 179       0       0       1      0.0025       0       0      14.545454545454543
    2.35      1.6     1.75 180       0       0       1      0.0025       0       0      14.805194805194803
    2.35     1.65     1.75 181       0       0       1      0.0025       0       0      15.064935064935064
    2.35      1.7     1.75 182       0       0       1      0.0025       0       0      15.324675324675324
    2.35     1.75     1.75 183       0       0       1      0.0025       0       0      15.584415584415583
    2.35      1.8     1.75 184       0       0       1      0.0025       0       0      15.844155844155843
    2.35     1.85     1.75 185       0       0       1      0.0025       0       0      16.103896103896
    2.35      1.9     1.75 186       0       0       1      0.0025       0       0      16.363636363636363
    2.35     1.95     1.75 187       0       0       1      0.0025       0       0      16.623376623376622
    2.35        2     1.75 188       0       0       1     0.00125       0       0      16.88311688311688
     2.4      1.5     1.75 189       0       0       1     0.00125       0       0      19.999999999999996
     2.4     1.55     1.75 190       0       0       1      0.0025       0       0      19.740259740259738
     2.4      1.6     1.75 191       0       0       1      0.0025       0       0      19.48051948051948
     2.4     1.65     1.75 192       0       0       1      0.0025       0       0      19.220779220779217
     2.4      1.7     1.75 193       0       0       1      0.0025       0       0      18.96103896103896
     2.4     1.75     1.75 194       0       0       1      0.0025       0       0      18.7012987012987
```

```
2.4    1.8    1.75 195    0    0    1    0.0025    0    0    18.44155844155844
2.4    1.85   1.75 196    0    0    1    0.0025    0    0    18.18181818181818
2.4    1.9    1.75 197    0    0    1    0.0025    0    0    17.92207792207792
2.4    1.95   1.75 198    0    0    1    0.0025    0    0    17.66233766233766
2.4    2      1.75 199    0    0    1    0.00125   0    0    17.4025974025974
2.45   1.5    1.75 200    0    0    1    0.00125   0    0    19.999999999999996
2.45   1.55   1.75 201    0    0    1    0.0025    0    0    20.25974025974026
2.45   1.6    1.75 202    0    0    1    0.0025    0    0    20.519480519480517
2.45   1.65   1.75 203    0    0    1    0.0025    0    0    20.77922077922078
2.45   1.7    1.75 204    0    0    1    0.0025    0    0    21.038961038961038
2.45   1.75   1.75 205    0    0    1    0.0025    0    0    21.298701298701296
2.45   1.8    1.75 206    0    0    1    0.0025    0    0    21.558441558441558
2.45   1.85   1.75 207    0    0    1    0.0025    0    0    21.818181818181817
2.45   1.9    1.75 208    0    0    1    0.0025    0    0    22.077922077922075
2.45   1.95   1.75 209    0    0    1    0.0025    0    0    22.337662337662337
2.45   2      1.75 210    0    0    1    0.00125   0    0    22.597402597402596
2.5    1.5    1.75 211    0    0    1    0.00125   0    0    25.71428571428571
2.5    1.55   1.75 212    0    0    1    0.0025    0    0    25.454545454545453
2.5    1.6    1.75 213    0    0    1    0.0025    0    0    25.19480519480519
2.5    1.65   1.75 214    0    0    1    0.0025    0    0    24.935064935064933
2.5    1.7    1.75 215    0    0    1    0.0025    0    0    24.675324675324674
2.5    1.75   1.75 216    0    0    1    0.0025    0    0    24.415584415584412
2.5    1.8    1.75 217    0    0    1    0.0025    0    0    24.155844155844154
2.5    1.85   1.75 218    0    0    1    0.0025    0    0    23.896103896103895
2.5    1.9    1.75 219    0    0    1    0.0025    0    0    23.636363636363633
2.5    1.95   1.75 220    0    0    1    0.0025    0    0    23.376623376623375
2.5    2      1.75 221    0    0    1    0.00125   0    0    23.116883116883116
2.55   1.5    1.75 222    0    0    1    0.00125   0    0    25.71428571428571
2.55   1.55   1.75 223    0    0    1    0.0025    0    0    25.97402597402597
2.55   1.6    1.75 224    0    0    1    0.0025    0    0    26.233766233766232
2.55   1.65   1.75 225    0    0    1    0.0025    0    0    26.49350649350649
2.55   1.7    1.75 226    0    0    1    0.0025    0    0    26.75324675324675
2.55   1.75   1.75 227    0    0    1    0.0025    0    0    27.01298701298701
2.55   1.8    1.75 228    0    0    1    0.0025    0    0    27.27272727272727
2.55   1.85   1.75 229    0    0    1    0.0025    0    0    27.53246753246753
2.55   1.9    1.75 230    0    0    1    0.0025    0    0    27.79220779220779
2.55   1.95   1.75 231    0    0    1    0.0025    0    0    28.05194805194805
2.55   2      1.75 232    0    0    1    0.00125   0    0    28.311688311688307
2.6    1.5    1.75 233    0    0    1    0.00125   0    0    31.428571428571427
2.6    1.55   1.75 234    0    0    1    0.0025    0    0    31.168831168831165
2.6    1.6    1.75 235    0    0    1    0.0025    0    0    30.909090909090907
2.6    1.65   1.75 236    0    0    1    0.0025    0    0    30.649350649350648
2.6    1.7    1.75 237    0    0    1    0.0025    0    0    30.389610389610386
2.6    1.75   1.75 238    0    0    1    0.0025    0    0    30.129870129870127
2.6    1.8    1.75 239    0    0    1    0.0025    0    0    29.87012987012987
2.6    1.85   1.75 240    0    0    1    0.0025    0    0    29.610389610389607
2.6    1.9    1.75 241    0    0    1    0.0025    0    0    29.35064935064935
2.6    1.95   1.75 242    0    0    1    0.0025    0    0    29.090909090909086
2.6    2      1.75 243    0    0    1    0.00125   0    0    28.831168831168828
2.65   1.5    1.75 244    0    0    1    0.00125   0    0    31.428571428571427
2.65   1.55   1.75 245    0    0    1    0.0025    0    0    31.688311688311686
2.65   1.6    1.75 246    0    0    1    0.0025    0    0    31.948051948051944
2.65   1.65   1.75 247    0    0    1    0.0025    0    0    32.2077922077922
2.65   1.7    1.75 248    0    0    1    0.0025    0    0    32.467532467532465
2.65   1.75   1.75 249    0    0    1    0.0025    0    0    32.72727272727273
2.65   1.8    1.75 250    0    0    1    0.0025    0    0    32.98701298701298
2.65   1.85   1.75 251    0    0    1    0.0025    0    0    33.246753246753244
2.65   1.9    1.75 252    0    0    1    0.0025    0    0    33.506493506493506
2.65   1.95   1.75 253    0    0    1    0.0025    0    0    33.76623376623376
2.65   2      1.75 254    0    0    1    0.00125   0    0    34.02597402597402
2.7    1.5    1.75 255    0    0    1    0.00125   0    0    37.14285714285714
2.7    1.55   1.75 256    0    0    1    0.0025    0    0    36.88311688311688
2.7    1.6    1.75 257    0    0    1    0.0025    0    0    36.62337662337662
2.7    1.65   1.75 258    0    0    1    0.0025    0    0    36.36363636363636
2.7    1.7    1.75 259    0    0    1    0.0025    0    0    36.1038961038961
2.7    1.75   1.75 260    0    0    1    0.0025    0    0    35.84415584415584
2.7    1.8    1.75 261    0    0    1    0.0025    0    0    35.58441558441558
2.7    1.85   1.75 262    0    0    1    0.0025    0    0    35.32467532467532
2.7    1.9    1.75 263    0    0    1    0.0025    0    0    35.064935064935064
2.7    1.95   1.75 264    0    0    1    0.0025    0    0    34.8051948051948
2.7    2      1.75 265    0    0    1    0.00125   0    0    34.54545454545454
2.75   1.5    1.75 266    0    0    1    0.00125   0    0    37.14285714285714
2.75   1.55   1.75 267    0    0    1    0.0025    0    0    37.4025974025974
2.75   1.6    1.75 268    0    0    1    0.0025    0    0    37.662337662337656
2.75   1.65   1.75 269    0    0    1    0.0025    0    0    37.92207792207792
2.75   1.7    1.75 270    0    0    1    0.0025    0    0    38.18181818181818
2.75   1.75   1.75 271    0    0    1    0.0025    0    0    38.441558441558435
```

2.75	1.8	1.75	272	0	0	1	0.0025	0	0	38.7012987012987
2.75	1.85	1.75	273	0	0	1	0.0025	0	0	38.96103896103896
2.75	1.9	1.75	274	0	0	1	0.0025	0	0	39.220779220779214
2.75	1.95	1.75	275	0	0	1	0.0025	0	0	39.480519480519476
2.75	2	1.75	276	0	0	1	0.00125	0	0	39.74025974025974
2.8	1.5	1.75	277	0	0	1	0.00125	0	0	42.857142857142854
2.8	1.55	1.75	278	0	0	1	0.0025	0	0	42.59740259740259
2.8	1.6	1.75	279	0	0	1	0.0025	0	0	42.33766233766234
2.8	1.65	1.75	280	0	0	1	0.0025	0	0	42.077922077922075
2.8	1.7	1.75	281	0	0	1	0.0025	0	0	41.8181818181818181
2.8	1.75	1.75	282	0	0	1	0.0025	0	0	41.55844155844156
2.8	1.8	1.75	283	0	0	1	0.0025	0	0	41.298701298701296
2.8	1.85	1.75	284	0	0	1	0.0025	0	0	41.038961038961034
2.8	1.9	1.75	285	0	0	1	0.0025	0	0	40.77922077922077
2.8	1.95	1.75	286	0	0	1	0.0025	0	0	40.51948051948052
2.8	2	1.75	287	0	0	1	0.00125	0	0	40.259740259740255
2.85	1.5	1.75	288	0	0	1	0.00125	0	0	42.857142857142854
2.85	1.55	1.75	289	0	0	1	0.0025	0	0	43.116883116883116
2.85	1.6	1.75	290	0	0	1	0.0025	0	0	43.37662337662337
2.85	1.65	1.75	291	0	0	1	0.0025	0	0	43.63636363636363
2.85	1.7	1.75	292	0	0	1	0.0025	0	0	43.896103896103895
2.85	1.75	1.75	293	0	0	1	0.0025	0	0	44.15584415584415
2.85	1.8	1.75	294	0	0	1	0.0025	0	0	44.41558441558441
2.85	1.85	1.75	295	0	0	1	0.0025	0	0	44.675324675324674
2.85	1.9	1.75	296	0	0	1	0.0025	0	0	44.93506493506493
2.85	1.95	1.75	297	0	0	1	0.0025	0	0	45.19480519480519
2.85	2	1.75	298	0	0	1	0.00125	0	0	45.45454545454545
2.9	1.5	1.75	299	0	0	1	0.00125	0	0	48.57142857142857
2.9	1.55	1.75	300	0	0	1	0.0025	0	0	48.31168831168831
2.9	1.6	1.75	301	0	0	1	0.0025	0	0	48.051948051948045
2.9	1.65	1.75	302	0	0	1	0.0025	0	0	47.79220779220779
2.9	1.7	1.75	303	0	0	1	0.0025	0	0	47.53246753246753
2.9	1.75	1.75	304	0	0	1	0.0025	0	0	47.272727272727266
2.9	1.8	1.75	305	0	0	1	0.0025	0	0	47.01298701298701
2.9	1.85	1.75	306	0	0	1	0.0025	0	0	46.75324675324675
2.9	1.9	1.75	307	0	0	1	0.0025	0	0	46.49350649350649
2.9	1.95	1.75	308	0	0	1	0.0025	0	0	46.23376623376623
2.9	2	1.75	309	0	0	1	0.00125	0	0	45.97402597402597
2.95	1.5	1.75	310	0	0	1	0.00125	0	0	48.57142857142857
2.95	1.55	1.75	311	0	0	1	0.0025	0	0	48.831168831168824
2.95	1.6	1.75	312	0	0	1	0.0025	0	0	49.090909090909086
2.95	1.65	1.75	313	0	0	1	0.0025	0	0	49.35064935064935
2.95	1.7	1.75	314	0	0	1	0.0025	0	0	49.6103896103896
2.95	1.75	1.75	315	0	0	1	0.0025	0	0	49.870129870129865
2.95	1.8	1.75	316	0	0	1	0.0025	0	0	50.12987012987013
2.95	1.85	1.75	317	0	0	1	0.0025	0	0	50.38961038961038
2.95	1.9	1.75	318	0	0	1	0.0025	0	0	50.649350649350644
2.95	1.95	1.75	319	0	0	1	0.0025	0	0	50.90909090909091
2.95	2	1.75	320	0	0	1	0.00125	0	0	51.16883116883116
3	1.5	1.75	321	0	0	1	0.00125	0	0	54.28571428571428
3	1.55	1.75	322	0	0	1	0.0025	0	0	54.02597402597402
3	1.6	1.75	323	0	0	1	0.0025	0	0	53.76623376623376
3	1.65	1.75	324	0	0	1	0.0025	0	0	53.5064935064935
3	1.7	1.75	325	0	0	1	0.0025	0	0	53.246753246753244
3	1.75	1.75	326	0	0	1	0.0025	0	0	52.98701298701298
3	1.8	1.75	327	0	0	1	0.0025	0	0	52.72727272727272
3	1.85	1.75	328	0	0	1	0.0025	0	0	52.467532467532465
3	1.9	1.75	329	0	0	1	0.0025	0	0	52.2077922077922
3	1.95	1.75	330	0	0	1	0.0025	0	0	51.94805194805194
3	2	1.75	331	0	0	1	0.00125	0	0	51.688311688311686
3.05	1.5	1.75	332	0	0	1	0.00125	0	0	54.28571428571428
3.05	1.55	1.75	333	0	0	1	0.0025	0	0	54.54545454545454
3.05	1.6	1.75	334	0	0	1	0.0025	0	0	54.8051948051948
3.05	1.65	1.75	335	0	0	1	0.0025	0	0	55.06493506493506
3.05	1.7	1.75	336	0	0	1	0.0025	0	0	55.32467532467532
3.05	1.75	1.75	337	0	0	1	0.0025	0	0	55.58441558441558
3.05	1.8	1.75	338	0	0	1	0.0025	0	0	55.844155844155836
3.05	1.85	1.75	339	0	0	1	0.0025	0	0	56.1038961038961
3.05	1.9	1.75	340	0	0	1	0.0025	0	0	56.36363636363636
3.05	1.95	1.75	341	0	0	1	0.0025	0	0	56.623376623376615
3.05	2	1.75	342	0	0	1	0.00125	0	0	56.88311688311688
3.1	1.5	1.75	343	0	0	1	0.000833332	0	0	59.99999999999999
3.1	1.55	1.75	344	0	0	1	0.00125	0	0	59.74025974025974
3.1	1.6	1.75	345	0	0	1	0.00125	0	0	59.480519480519476
3.1	1.65	1.75	346	0	0	1	0.00125	0	0	59.220779220779214
3.1	1.7	1.75	347	0	0	1	0.00125	0	0	58.96103896103896
3.1	1.75	1.75	348	0	0	1	0.00125	0	0	58.7012987012987

```
     3.1      1.8     1.75 349       0       0       1    0.00125       0       0      58.441558441558435
     3.1     1.85     1.75 350       0       0       1    0.00125       0       0      58.18181818181817
     3.1      1.9     1.75 351       0       0       1    0.00125       0       0      57.92207792207792
     3.1     1.95     1.75 352       0       0       1    0.00125       0       0      57.662337662337656
     3.1        2     1.75 353       0       0       1  0.000416666       0       0      57.402597402597394
123 134 124
135 124 134
124 135 125
136 125 135
125 136 126
137 126 136
126 137 127
138 127 137
127 138 128
139 128 138
128 139 129
140 129 139
129 140 130
141 130 140
130 141 131
142 131 141
131 142 132
143 132 142
132 143 133
144 133 143
134 145 135
146 135 145
135 146 136
147 136 146
136 147 137
148 137 147
137 148 138
149 138 148
138 149 139
150 139 149
139 150 140
151 140 150
140 151 141
152 141 151
141 152 142
153 142 152
142 153 143
154 143 153
143 154 144
155 144 154
145 156 146
157 146 156
146 157 147
158 147 157
147 158 148
159 148 158
148 159 149
160 149 159
149 160 150
161 150 160
150 161 151
162 151 161
151 162 152
163 152 162
152 163 153
164 153 163
153 164 154
165 154 164
154 165 155
166 155 165
156 167 157
168 157 167
157 168 158
169 158 168
158 169 159
170 159 169
159 170 160
171 160 170
160 171 161
172 161 171
161 172 162
173 162 172
```

```
162 173 163
174 163 173
163 174 164
175 164 174
164 175 165
176 165 175
165 176 166
177 166 176
167 178 168
179 168 178
168 179 169
180 169 179
169 180 170
181 170 180
170 181 171
182 171 181
171 182 172
183 172 182
172 183 173
184 173 183
173 184 174
185 174 184
174 185 175
186 175 185
175 186 176
187 176 186
176 187 177
188 177 187
178 189 179
190 179 189
179 190 180
191 180 190
180 191 181
192 181 191
181 192 182
193 182 192
182 193 183
194 183 193
183 194 184
195 184 194
184 195 185
196 185 195
185 196 186
197 186 196
186 197 187
198 187 197
187 198 188
199 188 198
189 200 190
201 190 200
190 201 191
202 191 201
191 202 192
203 192 202
192 203 193
204 193 203
193 204 194
205 194 204
194 205 195
206 195 205
195 206 196
207 196 206
196 207 197
208 197 207
197 208 198
209 198 208
198 209 199
210 199 209
200 211 201
212 201 211
201 212 202
213 202 212
202 213 203
214 203 213
203 214 204
215 204 214
204 215 205
```

```
216 205 215
205 216 206
217 206 216
206 217 207
218 207 217
207 218 208
219 208 218
208 219 209
220 209 219
209 220 210
221 210 220
211 222 212
223 212 222
212 223 213
224 213 223
213 224 214
225 214 224
214 225 215
226 215 225
215 226 216
227 216 226
216 227 217
228 217 227
217 228 218
229 218 228
218 229 219
230 219 229
219 230 220
231 220 230
220 231 221
232 221 231
222 233 223
234 223 233
223 234 224
235 224 234
224 235 225
236 225 235
225 236 226
237 226 236
226 237 227
238 227 237
227 238 228
239 228 238
228 239 229
240 229 239
229 240 230
241 230 240
230 241 231
242 231 241
231 242 232
243 232 242
233 244 234
245 234 244
234 245 235
246 235 245
235 246 236
247 236 246
236 247 237
248 237 247
237 248 238
249 238 248
238 249 239
250 239 249
239 250 240
251 240 250
240 251 241
252 241 251
241 252 242
253 242 252
242 253 243
254 243 253
244 255 245
256 245 255
245 256 246
257 246 256
246 257 247
258 247 257
```

247 258 248
259 248 258
248 259 249
260 249 259
249 260 250
261 250 260
250 261 251
262 251 261
251 262 252
263 252 262
252 263 253
264 253 263
253 264 254
265 254 264
255 266 256
267 256 266
256 267 257
268 257 267
257 268 258
269 258 268
258 269 259
270 259 269
259 270 260
271 260 270
260 271 261
272 261 271
261 272 262
273 262 272
262 273 263
274 263 273
263 274 264
275 264 274
264 275 265
276 265 275
266 277 267
278 267 277
267 278 268
279 268 278
268 279 269
280 269 279
269 280 270
281 270 280
270 281 271
282 271 281
271 282 272
283 272 282
272 283 273
284 273 283
273 284 274
285 274 284
274 285 275
286 275 285
275 286 276
287 276 286
277 288 278
289 278 288
278 289 279
290 279 289
279 290 280
291 280 290
280 291 281
292 281 291
281 292 282
293 282 292
282 293 283
294 283 293
283 294 284
295 284 294
284 295 285
296 285 295
285 296 286
297 286 296
286 297 287
298 287 297
288 299 289
300 289 299
289 300 290

301 290 300
290 301 291
302 291 301
291 302 292
303 292 302
292 303 293
304 293 303
293 304 294
305 294 304
294 305 295
306 295 305
295 306 296
307 296 306
296 307 297
308 297 307
297 308 298
309 298 308
299 310 300
311 300 310
300 311 301
312 301 311
301 312 302
313 302 312
302 313 303
314 303 313
303 314 304
315 304 314
304 315 305
316 305 315
305 316 306
317 306 316
306 317 307
318 307 317
307 318 308
319 308 318
308 319 309
320 309 319
310 321 311
322 311 321
311 322 312
323 312 322
312 323 313
324 313 323
313 324 314
325 314 324
314 325 315
326 315 325
315 326 316
327 316 326
316 327 317
328 317 327
317 328 318
329 318 328
318 329 319
330 319 329
319 330 320
331 320 330
321 332 322
333 322 332
322 333 323
334 323 333
323 334 324
335 324 334
324 335 325
336 325 335
325 336 326
337 326 336
326 337 327
338 327 337
327 338 328
339 328 338
328 339 329
340 329 339
329 340 330
341 330 340
330 341 331
342 331 341

```
332 343 333
344 333 343
333 344 334
345 334 344
334 345 335
346 335 345
335 346 336
347 336 346
336 347 337
348 337 347
337 348 338
349 338 348
338 349 339
350 339 349
339 350 340
351 340 350
340 351 341
352 341 351
341 352 342
353 342 352

ZONE F=FEPOINT, N=4, NV=4, E=2, ET=TRIANGLE, T=BACKING
     2.1      1.5     1.65 354       0       0      -1   0.166667       0       0       0
     3.1      1.5     1.65 355       0       0      -1   0.0833333      0       0       0
     3.1       2     1.65 356       0       0      -1   0.166667       0       0       0
     2.1       2     1.65 357       0       0      -1   0.0833333      0       0       0
354 356 355
354 357 356

ZONE F=FEPOINT, N=4, NV=4, E=2, ET=TRIANGLE, T=BACKING
     2.1      1.5     1.65 354      -1       0       0   0.0166667      0       0       0
     2.1       2     1.65 357      -1       0       0  0.00833334      0       0       0
     2.1      1.5     1.75 358      -1       0       0  0.00833334      0       0       0
     2.1       2     1.75 361      -1       0       0   0.0166667      0       0       0
361 354 358
357 354 361

ZONE F=FEPOINT, N=4, NV=4, E=2, ET=TRIANGLE, T=BACKING
     3.1      1.5     1.65 355       1       0       0   0.0166667      0       0       0
     3.1       2     1.65 356       1       0       0  0.00833334      0       0       0
     3.1      1.5     1.75 359       1       0       0  0.00833334      0       0       0
     3.1       2     1.75 360       1       0       0   0.0166667      0       0       0
359 355 360
360 355 356

ZONE F=FEPOINT, N=4, NV=4, E=2, ET=TRIANGLE, T=BACKING
     2.1      1.5     1.65 354       0      -1       0   0.0333333      0       0       0
     3.1      1.5     1.65 355       0      -1       0   0.0166667      0       0       0
     2.1      1.5     1.75 358       0      -1       0   0.0166667      0       0       0
     3.1      1.5     1.75 359       0      -1       0   0.0333333      0       0       0
359 354 355
358 354 359

ZONE F=FEPOINT, N=4, NV=4, E=2, ET=TRIANGLE, T=BACKING
     3.1       2     1.65 356       0       1       0   0.0333333      0       0       0
     2.1       2     1.65 357       0       1       0   0.0166667      0       0       0
     3.1       2     1.75 360       0       1       0   0.0166667      0       0       0
     2.1       2     1.75 361       0       1       0   0.0333333      0       0       0
356 361 360
356 357 361

ZONE F=FEPOINT, N=4, NV=4, E=2, ET=TRIANGLE, T=SW
      0        0      3.5 362       0       0      -1    5.36667       0       0       0
     4.6       0       3.5 363      0       0      -1    2.68333       0       0       0
     4.6      3.5       3.5 364      0       0      -1    5.36667       0       0       0
      0       3.5      3.5 365      0       0      -1    2.68333       0       0       0
362 364 363
362 365 364
```